NATIONAL ADVISORY COMMITTEE FOR AERONAUTICS

TECHNICAL NOTE 2944

THE ZERO-LIFT DRAG OF A SLENDER BODY OF REVOLUTION (NACA RM-10 RESEARCH MODEL) AS DETERMINED FROM TESTS IN SEVERAL WIND TUNNELS AND IN FLIGHT AT SUPERSONIC SPEEDS

By Albert J. Evans

NACA Headquarters

Washington
April 1953

1D

NATIONAL ADVISORY COMMITTEE FOR AERONAUTICS

TECHNICAL NOTE 2944

THE ZERO-LIFT DRAG OF A SLENDER BODY OF REVOLUTION (NACA RM-10 RESEARCH MODEL) AS DETERMINED FROM TESTS IN SEVERAL WIND TUNNELS AND IN FLIGHT AT SUPERSONIC SPEEDS

By Albert J. Evans

SUMMARY

The results of tests of a slender body of revolution designated the NACA RM-10 have been compiled from various NACA test facilities.

Zero-lift drag data are presented for a Reynolds number range from about 1×10^6 to 40×10^6 from several wind tunnels and from about 12×10^6 to 140×10^6 from free-flight tests. The Mach numbers covered include 1.5 to 2.4 for the wind-tunnel data and 0.85 to 2.5 for the flight results. The wind-tunnel models were tested with and without 60° sweptback stabilizing fins and the flight models were tested with stabilizing fins.

Comparison of the data obtained in the several wind tunnels for the body alone (without fins) shows good agreement between the different facilities. There are unexplained differences however between the wind-tunnel results with fins attached and flight results, as well as differences between full-scale and half-scale flight models, which cannot be explained as an effect of Reynolds number.

The results presented are compiled in the present paper to facilitate the correlation of results obtained in other test facilities.

INTRODUCTION

During the early development period of wind-tunnel testing, it was found that test data from different wind tunnels frequently showed important discrepancies. Many of these difficulties were resolved by a combination of improved techniques and equipment, together with the application of wall and support interference corrections. In an effort to reduce further the uncertainty of comparisons between data from

various sources, it was considered desirable to make tests of the same model in many different wind tunnels. In 1920 the British Aeronautical Research Committee instituted a program of international scope (ref. 1) whereby the same NPL airship and wing models were tested in the major facilities of the world.

Since that time the subsonic wind tunnel has become a reliable source of aerodynamic data, and the reasons for the discrepancies that remain are fairly well understood. In recent years many supersonic wind tunnels have been built, and the test results have shown in some cases a lack of agreement too large to be ignored. An interest has accordingly been expressed in a test program for the supersonic speed range similar to the early subsonic program.

During the December 1952 Rome meeting of the Advisory Group for Aeronautical Research and Development of the North Atlantic Treaty Organization, it was decided to encourage such a program of tests in supersonic wind tunnels. One configuration selected for this purpose was a slender body of revolution designated the NACA RM-10, for which the zero-lift drag had been measured in several NACA wind tunnels and in flight.

The purpose of the present paper is to compile and present the results of the drag measurements from the various test facilities and to make the results generally available in a concise form to those who would be interested in making comparable tests in other test facilities.

The present paper presents a brief description of the model installation in each of the test facilities together with a description of the model instrumentation and the methods used to reduce the measured data to drag-coefficient form.

The results presented cover a Reynolds number range from about 12×10^6 to 140×10^6 for the free-flight models and 1×10^6 to 40×10^6 for the tunnel models. The Mach numbers covered include 0.85 to 2.5 in flight and about 1.5 to 2.4 in the wind tunnels.

The results presented herein have been gathered from a number of independent NACA investigations and in some cases descriptive material, sketches, or descriptions of data-reduction procedure are credited to the original investigators. The following list contains the names of NACA staff members whose work has been presented herein.

L. E. Hasel
A. R. Sinclair
C. V. Hamilton
K. R. Czarnecki
J. E. Marte

} 4- by 4-foot tunnel
Langley Aeronautical Laboratory

R. W. Luidens P. C. Simon F. T. Esenwein L. J. Obery C. F. Schueller	8- by 6-foot tunnel Lewis Flight Propulsion Laboratory
E. S. Love D. E. Colletti A. E. Bromm	9-inch tunnel Langley Aeronautical Laboratory
E. F. Perkins F. E. Gowen L. H. Jorgensen	1- by 3-foot tunnel, No. 2 Ames Aeronautical Laboratory
H. H. Jackson C. B. Rumsey L. T. Chauvin J. D. Loposer	Rocket propelled model tests Pilotless Aircraft Research Division Langley Aeronautical Laboratory

SYMBOLS

A	body frontal area
C_{D_B}	base drag coefficient, D_B/qA
C_{D_f}	forebody friction drag coefficient, D_f/qA
C_{D_P}	forebody pressure drag coefficient, D_P/qA
C_{D_T}	total drag coefficient with or without fins, D_T/qA
c_p	specific heat at constant pressure, 7.74 Btu/lb/$^\circ$F for air
D_b	body base diameter
D_s	sting or sting shield diameter
g	acceleration due to gravity, 32.2 ft/sec/sec
J	mechanical equivalent of heat, 778 ft-lb/Btu
L	basic body length

M	Mach number
q	dynamic pressure, $\frac{1}{2}\rho V^2$, lb/sq ft
r	radial distance from body axis to any point in boundary layer
r_w	radial distance from body axis to body surface
R	Reynolds number
s	distance from nose to any point on body surface
T_{aw}	adiabatic wall temperature, $^{\circ}F$ abs
T_s	stagnation temperature, $^{\circ}F$ abs
T_δ	temperature just outside boundary layer, $^{\circ}F$ abs
T_w	temperature at body skin, $^{\circ}F$ abs
t/c	ratio of maximum fin thickness to fin chord perpendicular to leading edge
u	velocity inside boundary layer, ft/sec
U_δ	velocity just outside boundary layer, ft/sec
V	free-stream velocity, ft/sec
x	axial distance from nose to any point on body axis
y	normal distance from body skin to any point in boundary layer
α	angle of attack, deg
ρ	free-stream density, slugs/cu ft
ρ_δ	air density just outside boundary layer, slugs/cu ft
τ_w	wall shearing stress, lb/sq ft

APPARATUS AND RANGE OF TESTS

RM-10 Missile

A sketch of the RM-10 missile, giving the important model dimensions as a fraction of basic body length, is presented in figure 1. The profile of the body is such that its meridians are parabolic arcs whose coordinates are given by the equation $r_w = \frac{x}{7.5}\left(1.0 - \frac{x}{L}\right)$. The basic fineness ratio of the body is 15. To provide for the rocket jet, however, the base was cut off at the 81.33-percent-length station, which resulted in a fineness ratio of 12.2. The four stabilizing fins, spaced equally around the stern, had an untapered plan form. The fins were swept back 60° and incorporated 10-percent-thick circular-arc airfoil sections normal to the leading edge.

Most of the wind-tunnel tests were made on the body alone (without tail fins); however, fins were added in some of the tunnel tests to afford a comparison with the results of flight tests.

Details of the models tested in the various test facilities and in flight are presented under the description of the test setup in each test facility. Some of the pertinent model details are also presented in table I.

Figure 2 shows the details of the base sections of the various tunnel models and the details of the flight-model bases are shown in figure 3.

4- by 4-Foot Supersonic Tunnel and Model

The Langley 4- by 4-foot tunnel is a rectangular, closed-throat, single-return-type, variable-density wind tunnel. The results of the tests reported herein were obtained on three models one of which was 50 inches in length and two were 42.05 inches long.

The 50-inch model was sting mounted in the tunnel test section (see figs. 2(a) and 4(a)) and was used to measure total body drag, base pressure drag, and skin friction drag.

The 42.05-inch models were also sting mounted and were used to obtain the body pressure drag, and total and base drag of the body with fins installed.

Model construction.- The 50-inch model was constructed of steel and Duralumin in four sections. The original surface roughnesses were about

6 root-mean-square microinches on the steel and about 14 root-mean-square microinches on the Duralumin parts with maximum peak-to-valley roughnesses of 12 and 50 microinches, respectively. Most of the tests were made, however, with the model painted, sanded, waxed, and polished so that the resulting surface roughness was less than those of the original surface.

One of the 42.05-inch models was constructed to produce a light-weight model for some special wire-supported tests which are not included herein. This model, however, was also tested as a sting-supported model with tail fins attached and the results of these force tests are reported in the present paper.

The midsection of the light 42.05-inch force model was formed by gluing a 1/4-inch-thick layer of balsa wood around a load-carrying structure. The balsa wood was then wrapped with glass-fiber cloth and impregnated with a thermosetting plastic which was stable and readily machined. Magnesium nose and base sections were attached to the built-up midsection. This model was used to obtain drag data with fins attached to the body. The four fins were machined from magnesium.

The other 42.05-inch model was constructed of steel and was used to obtain the pressure drag of the model forebody.

Model instrumentation.- The force-measurement models were sting mounted and the total drag was measured on an electrical strain-gage balance mounted within the model (fig. 4(a)). Base pressures were measured by four tubes placed on the sting with the openings in the plane of the base at 90° intervals around the sting (fig. 2(a)). Boundary-layer profiles were determined by means of a rake shown in figure 2(a). The rake was clamped to the sting so that boundary-layer profiles were determined about 1/64 inch ahead of the model base. For the boundary-layer-profile measurements the base of the model was blocked rigidly against the sting with wooden wedges to prevent any relative movement between the model and the rake. No other measurements were made during these tests.

Forebody pressure drag was determined from the forebody longitudinal pressure distribution which was measured by 140 orifices located in 4 rows 90° apart.

For some of the tests conducted in the 4- by 4-foot tunnel data were obtained with the boundary-layer transition point fixed near the model nose. In this case transition was fixed by means of a circumferential ring of No. 60 carborundum grains located 1/2 inch back from the model nose and about 1/4 inch wide in the direction of flow.

The ratio of the sting to base diameter for the 50-inch model was 0.579. This ratio for the 42.05-inch force and pressure models was 0.36 and 0.60, respectively.

Range of tests.- Total drag of the body, base drag, and the body skin friction drag were measured on the 50-inch model at a Mach number of 1.6 for a range of Reynolds number from 2×10^6 to 40×10^6. The tests were made at zero angle of attack with natural and fixed transition without tail fins attached.

The tests with the 42.05-inch body consisted of measurement of the forebody pressure distribution at a Mach number of 1.59 for Reynolds numbers between 1.8×10^6 and 4.5×10^6. The 42.05-inch model was also tested with tail fins attached.

8- by 6-Foot Supersonic Tunnel and Model

The Lewis 8- by 6-foot tunnel is a rectangular, closed-throat, nonreturn-type wind tunnel. The results reported herein were obtained on two models which had body lengths of 73 inches. One model was used to obtain strain-gage measurements of total drag and was instrumented to obtain base pressure measurements with and without the stabilizing fins attached. The second model was used to obtain the forebody pressure drag and skin friction drag.

Model construction.- The model bodies were spun from aluminum sheet and the noses of the bodies were blunted by removing 1/4 inch from the pointed tip. There was some deviation of the actual pressure-model contour from the calculated dimensions of the model. The deviation was relatively large (0.032 inch undersize) at a station 20 inches behind the model nose and was of the order of 0.01 inch over the remainder of the body except for a small portion near the base which was 0.02 inch undersize. No surface roughness measurements are available for these models.

Model instrumentation.- One model was rigidly connected to a three-component strain-gage balance located inside the body and the balance was attached to the tunnel sting-strut combination (fig. 4(a)). The strain-gage balance measured the total drag of the model.

Base pressure was measured at orifices on the model base located at $\pm 45^\circ$ to each of the rows of body surface pressure orifices and at a radius of 1.624 inches as shown in figure 2(b).

The pressure model was sting mounted on an internal cam mechanism which allowed the model to be remotely rotated to determine the circumferential variation of the pressure distribution.

The forebody pressure drag was determined from the pressure distribution measured by two diametrically opposite rows of pressure orifices consisting of 23 orifices each.

Boundary-layer profiles were determined by diametrically opposite rakes extending $1\frac{3}{4}$ inches into the stream in the plane of the model base.

The ratio of sting to base diameter was 0.66.

Range of tests.- The tests were conducted at values of Reynolds number of 29.1, 29.2, 29.5, and 31.1×10^6 for Mach numbers of 1.49, 1.59, 1.78, and 1.98, respectively.

9-Inch Supersonic Tunnel and Model

The Langley 9-inch tunnel is a rectangular, closed-throat, closed-circuit-type, variable-density wind tunnel. The models tested had over-all body lengths of 9 inches and 7.325 inches.

Model construction.- Three models, two of which were identical except for construction details, were tested in the 9-inch tunnel.

The measured ordinates of the models were within 0.001 inch of the calculated contour, and the surface roughness of the model was 5 root-mean-square microinches. These two models were 9 inches in length.

A third model, 7.325 inches long, was constructed to incorporate tail fins.

Model instrumentation.- Total drag measurements were made with a strain-gage balance located in the sting support external of the model as shown in figure 4(b). The sting support was shielded to eliminate any tare forces on the sting. The shield extended just inside the model base, as shown in figure 2(c), and was arranged so that the pressure inside the balance housing was equal to the model base pressure, permitting the determination of the model base pressure by measurement of the pressure inside the balance housing.

Boundary-layer-profile measurements were made by means of a probe mounted through the tunnel wall.

Forebody pressure drag was determined from the longitudinal pressure distributions which were measured by a single row of 27 orifices. A distribution of pressure around the model was obtained by rotating the model about its longitudinal axis.

Some of the tests were run with the boundary-layer transition fixed near the nose of the model (9-inch model). Transition was fixed by placing carborundum strips as near the body nose as possible. These strips were 3/16 inch wide and in one case the strip was 0.007 inch thick using No. 180 carborundum grains and in another case was 0.017 inch thick when No. 60 grains were used. The data showed that the thin strip caused transition satisfactorily and also showed that perhaps the drag of the larger grains affected the drag results. As a consequence only the thin-strip data have been included herein. The 7.325-inch model (with tail fins) was tested with natural transition.

The ratio of sting to base diameter for the 9-inch models was 0.589, and that for the 7.325-inch model, 0.49.

Range of tests.- The tests on the body without tail fins were conducted at Mach numbers of 1.62, 1.93, and 2.41 over a Reynolds number range of approximately 1×10^6 to 11×10^6 at each Mach number.

The tests with fins attached to the 7.325-inch body were conducted at a Mach number of 1.62 and a Reynolds number of 2.66×10^6.

1- by 3-Foot Supersonic Tunnel and Model

The Ames 1- by 3-foot tunnel No. 2 is an intermittent blow-down wind tunnel. The model tested in the 1- by 3-foot tunnel was 12.208 inches in over-all body length.

Model instrumentation.- The total drag of the model was measured by an electrical strain-gage balance mounted in the sting support external to the model. The sting support was shielded to eliminate any tare forces on the sting (see fig. 2(d)) and was arranged so that the pressure inside the balance housing was equal to the model base pressure, permitting the determination of the model base pressure by measurement of the pressure inside the balance housing.

Skin friction drag was obtained in the 1- by 3-foot-tunnel investigation indirectly by subtracting the forebody pressure and base drag from the total drag.

Measurements of the body surface roughness are not available for the 1- by 3-foot-tunnel model. Forebody pressure drag was determined from the longitudinal pressure distribution on the body, which was measured by a single row of 12 orifices. The circumferential pressure variation was measured by rotating the body.

The tests conducted in the 1- by 3-foot tunnel were made with natural transition.

Range of tests.- The tests were conducted at Reynolds numbers of 8.6 and 17.4 $\times 10^6$ and for Mach numbers of 1.52 and 1.98 for the body alone and 1.98 for the body with tail fins.

Flight Models

The results obtained in free flight were obtained on nine rocket-powered models of the same configuration. Five of the models were 146.5 inches in over-all body length and are designated as flight models 1, 5, 6, 7, and 8. Model 1 was used to obtain base pressure measurements and models 5, 6, 7, and 8 were used to obtain the total drag measurements. The other four models were 73.25 inches in length and are designated as models A, B, C, and E.

Model construction.- The models were all metal in construction, utilizing spun magnesium-alloy skins and cast magnesium-alloy tail cones to which the tail fins were attached.

All models carried a sustainer motor internally; one 146.5-inch model and all the 73.25-inch models also utilized various booster rocket motors to obtain high Mach numbers.

The body coordinates of the models were within 0.020 inch of the computed body contour and the surfaces were smooth and highly polished at the time of launching.

Model instrumentation.- The data presented for the flight models were obtained during the decelerating portion of the flight trajectory after rocket-motor burnout.

Velocity and total drag were obtained from the CW Doppler radar. Also, total drag and base drag were reduced from data telemetered to the ground receiving station by instrumentation incorporating a longitudinal accelerometer and a pressure cell. Atmospheric data were obtained by radiosonde observations.

Base pressure was measured inside the afterbody between the rocket nozzle and the skin by an open-end tube located in the models as shown in figure 3.

Range of tests.- The Mach number range was from approximately 0.85 to 2.5 and the Reynolds number range was from 12 $\times 10^6$ to 140 $\times 10^6$.

DATA REDUCTION

Total drag.- Total drag is defined as the drag of the models with or without fins as determined from measurements obtained from the strain-gage balance in the case of the wind-tunnel model tests. The total drag of the flight models was determined from measurements of the model deceleration after rocket-motor burnout by Doppler radar and telemeter apparatus.

Base drag.- Base drag was determined from pressure measurements made at the base of the models. The position of the pressure orifice at the base of each of the models is shown in figures 2 and 3. Base drag is defined as the difference between the pressure measured on the model base and the free-stream static pressure times the model base area.

Forebody pressure drag.- Forebody pressure drag is defined as the axial force exerted on the model body by the pressures acting on the model surface excluding the model base surface. The value of forebody pressure drag was determined by integrating the measured pressure distribution over the body surface with respect to the body frontal area.

Skin friction drag.- Skin friction drag coefficients were determined by means of rake surveys of the total pressure through the boundary layer and static-pressure measurements at the rake location. Skin friction drag was determined in the 1- by 3-foot tunnel by subtracting the base and forebody pressure drag from the model total drag. Results from the 4- by 4-foot and 9-inch tunnels were obtained by both rake surveys and subtraction.

Reduction of the rake pressure measurements to obtain skin friction drag requires a knowledge of the temperature through the boundary layer which was determined by using the theoretical relation given by Crocco in reference 2 which gives the temperature as a function of velocity. This relation, which assumes a Prandtl number of 1.0 and steady-state conditions, was modified by the inclusion of the recovery factor β in order to obtain adiabatic wall temperature rather than stagnation temperature when the heat transfer is zero. The relation used is then

$$T = a + bu - \frac{\beta u^2}{2Jgc_p}$$

where $\beta = \frac{T_{aw} - T_\delta}{T_s - T_\delta}$ and a and b are constants.

Evaluating the constants from the boundary conditions, $T = T_\delta$ at $u = U_\delta$ and $T = T_u$, and introducing the definition of adiabatic wall temperature

$$T_{aw} = T_\delta + \frac{\beta U_\delta^2}{2Jgc_p}$$

give

$$T = T_\delta + \left(T_w - T_{aw}\right)\left(1 - \frac{u}{U_\delta}\right) + \frac{\beta\left(U_\delta^2 - u^2\right)}{2Jgc_p}$$

A value of $\beta = 0.88$, an approximation for both laminar and turbulent boundary layers, was used in the reduction of the 4- by 4-foot-tunnel data. The results from the 9-inch tunnel were obtained by using a value of $\beta = 0.88$ for laminar flow and $\beta = 1.0$ for turbulent boundary-layer flow.

The integrated form of the boundary-layer equation from reference 3 can be written as

$$\tau_w r_w = \frac{d}{ds}\int_0^\delta \left(\rho_\delta U_\delta^2 - \rho u^2\right) r \, dy - U_\delta \frac{d}{ds}\int_0^\delta \left(\rho_\delta U_\delta - \rho u\right) r \, dy$$

By taking $dx = ds$, which causes negligible error for a slender body of revolution, letting $r = r_w + y$, and integrating with respect to x, the average skin friction drag coefficient is given by

$$C_{D_f} = \frac{2\pi}{qA}\int_0^x \tau_w r_w \, dx$$

The variation of boundary-layer thickness with axial distance along the body was assumed to be linear from a value of 0 at the body nose to the value determined at the measurement station. This estimation of the boundary-layer growth was used in the determination of the skin friction drag coefficients from the 4- by 4-foot-tunnel and 8- by 6-foot-tunnel tests. The error involved in using this assumption of linear boundary-layer growth amounts to less than 5 percent of the skin friction drag coefficient. The coefficients from the 9-inch-tunnel pressure surveys have been determined from a calculation of the boundary-layer growth along the body.

Force coefficients.- All the force coefficients presented herein are based on the free-stream dynamic pressure and the maximum cross-sectional area of the body.

Corrections.- The wind-tunnel data presented herein have been corrected for the buoyancy effects on the drag coefficients in all cases where the corrections were required. In some of the tunnel tests the static-pressure gradient through the tunnel test section was sufficiently small that the corrections to the drag values fell well within the experimental accuracy of the data. In these cases no buoyancy corrections were applied to the drag data.

The results of investigations to determine the effects of sting diameter and length of sting behind a boattailed body have shown that sting interference effects are negligible for the ratios of sting to base diameter and of length of sting to base diameter used in the present tests. Sting interference corrections are therefore not necessary for the data presented herein.

The results of the wind-tunnel tests presented were obtained in all cases under conditions of temperature equilibrium between the model body and free stream.

Also in all cases condensation-free flow was maintained during the tests.

RESULTS AND DISCUSSION

Presentation of results.- The results of the drag tests in the various wind tunnels and in flight are presented in figures 5 to 9. All the results are presented for zero angle of attack and are presented as plots of C_{D_T}, C_{D_B}, C_{D_p}, and C_{D_f} against either Mach number or Reynolds number depending on which quantity was varied during the tests. The symbols in figures 5 to 9 indicate the test points obtained in the various facilities. Figures 5 to 7 present the results of the wind-tunnel tests of the body with no fins attached for the condition of natural smooth-body boundary-layer transition and for transition fixed near the body nose. The forebody pressure drag coefficients presented in figure 5 were determined from measurements made on the 42.05-inch body in the 4- by 4-foot tunnel at relatively low Reynolds numbers for conditions of laminar and turbulent boundary layers. The values of forebody pressure drag coefficient determined from these tests were 0.041 for a laminar boundary layer and 0.044 for a turbulent boundary layer attained by fixing transition near the model nose. The values of forebody pressure drag coefficient presented are based on the assumption

that the values did not vary with Reynolds number except to change from laminar to turbulent values in the Reynolds number range near 10×10^6. This range was chosen on the basis of skin friction and boundary-layer-profile results. In actuality the transition in forebody pressure drag coefficient will not be so abrupt as assumed, but the difference between the coefficients is very small.

Values of total and base drag coefficient from the wind-tunnel tests for the body with four fins attached are presented in figure 8. The tests of the model with fins attached were conducted with natural transition.

In the case of the flight tests where Reynolds number and Mach number varied simultaneously during the tests the variation of Reynolds number with Mach number is presented in figure 10 for the nine models tested. Three curves are shown for the 146.5-inch models, two depicting the variation for the unboosted models 1, 5, 6, 7, and 8 and the third for the boosted model 6. The three curves shown for the 73.25-inch models represent differences in the three types of booster rockets used for the tests. The values of Reynolds number attained in the wind-tunnel tests of the model with fins, which were considerably lower for the 4- by 4-foot- and 9-inch-tunnel tests than the values for the body-alone tests, are spotted on the flight curves of figure 10 to afford a ready comparison of the range covered in the flight tests and the wind-tunnel tests.

Comparison and discussion of results.- The results of the tests in the several wind tunnels have been compared in figures 11 and 12 for conditions of natural and fixed transition with no fins attached to the body. The drag components are compared in figure 11 for two values of Mach number, namely, 1.6 and 1.93, for a range of Reynolds number. Figure 12 shows a comparison of the results for three values of Reynolds number, 3×10^6, 8.6×10^6, and 30×10^6, for a range of Mach number. The values of Mach number and Reynolds number chosen for the comparative plots were selected as values which afford the opportunity of comparing the majority of the data.

The results of the flight tests and of the tunnel tests with fins attached to the body are compared in figure 13 as a plot of total and base drag coefficient against Mach number. The flight data are presented as a band, the extremities of which are the extremities of the data presented in figure 9. Cross hatching has been used to distinguish the results of the 146.5-inch-model tests from those of the 73.25-inch-model tests.

Comparison of the wind-tunnel data for the body alone in figures 11 and 12 shows excellent agreement in the high Reynolds number range

between the data from the 8- by 6-foot tunnel and the 4- by 4-foot tunnel. In the low Reynolds number range the agreement in the trend of the data from the 9-inch- and 4- by 4-foot-tunnel results as shown in figure 11(a) is good although there are small discrepancies in the drag values obtained in the two facilities. With respect to the 9-inch-tunnel results the total drag values from the 4- by 4-foot tunnel are lower for both natural and fixed transition. Neglecting the differences in the indicated Reynolds number of transition between the two tunnels the magnitudes of the base drag results are in good agreement. No suitable explanation has been found for the differences in magnitude of the total drag results. The comparison of skin friction values in the laminar range shows, in general, good agreement.

The friction drag results shown in figure 11 for the 1- by 3-foot tunnel indicate that boundary-layer transition in this facility apparently occurred at much lower Reynolds numbers than in the 4- by 4-foot- or 9-inch-tunnel tests. This discrepancy can probably be attributed to the differences in wind-tunnel turbulence levels.

The variation of skin friction drag from the 9-inch tunnel with Mach number at constant values of Reynolds number of 3×10^6 and 8.6×10^6, shown in figures 12(a) and 12(b), shows a rise in skin friction drag coefficient with increasing Mach number for the body with natural transition. The rise in skin friction drag coefficient with Mach number shown in figure 12(a) for a Reynolds number of 3.0×10^6 is slight and is within the experimental accuracy of the tests. The steeper rise in friction drag coefficient shown in figure 12(b) for a Reynolds number of 8.6×10^6 can be attributed to the forward movement of the transition point with increasing Mach number which is evident from a comparison of the results presented in figures 7(a), 7(c), and 7(e). These figures show that the transition Reynolds number was approximately 8.8, 7.5, and 6.0×10^6 for Mach numbers of 1.62, 1.93, and 2.41, respectively. The effect of increasing Mach number in decreasing the Reynolds number of transition is appreciable but is in agreement with theoretical results concerning boundary-layer stability for the case of zero heat transfer between the body and the air stream.

A comparison of the test results for the two different-sized flight models is shown in figure 13. The results of tunnel tests with fins attached to the body are also shown in figure 13 for comparison with the flight results.

As shown in figure 10 the Reynolds number range for the smaller 73.25-inch model is for the most part contained within the range for the larger 146.5-inch models. Therefore, the differences in the drag coefficients for the two sizes of models shown in figure 13 are not readily explainable on the basis of Reynolds number.

Examination of the base drag results in figure 13 shows that the base drag of the smaller models is about half that for the larger flight model and that this difference accounts almost completely for the difference in total drag for the two sets of flight data. It does not appear likely that these differences are due to an error in measurement since the total drag and base drag were measured independently. Furthermore, the smaller model results were obtained from several separate flights and the larger model base drag results agree with values obtained in three different wind tunnels. This latter agreement would be expected since the boundary layer at the base was probably turbulent for all these models because of the presence of the fins. The base drag for the smaller flight models appears to be low for some as yet unknown reason.

The total drag as measured in the 8- by 6-foot-tunnel tests appears to agree closely with the drag of the larger flight models at $M = 1.5$, but this may be fortuitous in view of the differences in Reynolds numbers. It has been suggested that the differences in slope of the 8- by 6-foot-tunnel and the flight drag curves may be explained by the fact that the Reynolds number of the 8- by 6-foot-tunnel tests was essentially constant while that of the flight models increased with increasing Mach number. This does not seem correct, however, since the Reynolds number range obtained on several models at a given Mach number is considerably larger than the Reynolds number change in going from Mach number 1.5 for example to 2.0. If the total drag of the smaller flight models were adjusted by the amount required to bring the base drag into agreement with that for the larger model, it would bear the same relationship to the 8- by 6-foot-tunnel total drag results as do the drag data for the larger models.

The discrepancies noted in the foregoing discussion could possibly be due to behavior of the fin drag as influenced both by Mach number and Reynolds number. There is insufficient information available, however, to allow any conclusions to be drawn regarding this possibility.

With regard to the data in figure 13 from the 4- by 4-foot tunnel and the 9-inch tunnel it can be noted that the data for the models with fins were obtained at Reynolds numbers low enough to permit laminar flow over most of the body. The total drag would thus be expected to be lower than that for the other models which were tested at much larger Reynolds numbers. The agreement that apparently exists between the total drag data from these two tunnels and the data for the smaller flight models must therefore be regarded as fortuitous.

CONCLUDING REMARKS

The results of an extensive investigation, one objective of which was to form a basis for comparison of test results from various test facilities, have been compiled and are presented in the present paper for the purpose of making the data available to other research agencies interested in correlation of the results obtained in their test facilities with those obtained in NACA test facilities.

From comparison of the data obtained in NACA facilities it is observed that for the body alone (without tail fins) the total and component drag coefficients measured in the several wind tunnels were in good agreement when proper consideration is given to the state of the body boundary layer. Free-flight results on the finned models show a consistent discrepancy between two groups of models of different size. This discrepancy is undoubtedly due to a real difference in drag between the two groups of models but is not explainable with the information available. There are also observed certain differences between wind-tunnel and flight results which cannot be completely accounted for at present.

NACA Headquarters,
Washington, D. C., April 16, 1953.

REFERENCES

1. Anon.: Report on Aerofoil Tests at National Physical Laboratory and Royal Aircraft Establishment. R. & M. No. 954, British A.R.C., May 1925.

2. Crocco, Luigi: Transmission of Heat From a Flat Plate to a Fluid Flowing at a High Velocity. NACA TM 690, 1932.

3. Fluid Motion Panel of the Aeronautical Research Committee and Others (S. Goldstein, ed.): Modern Developments in Fluid Dynamics. Vol. I. The Clarendon Press (Oxford), 1938, p. 133.

TABLE I

RM-10 TEST CONFIGURATIONS

Tunnel size	Model length, in.	Model surface	Surface roughness	Fins	Type support
8 by 6 foot	73	Aluminum	Not available	Yes and no	Sting
4 by 4 foot	50	Steel and Duralumin in four sections	Painted, sanded, waxed and polished	No	Sting
	42.05	Plastic on glass fiber with magnesium nose, base and fins	Not available	Yes	
	42.05	Steel	Not available	No	
9 inch	9	Steel	5 rms μ in.	No	Sting
	7.325	Steel		Yes	
1 by 3 foot	12.2	---	Not available	Yes and no	Sting
Flight	146.5	Magnesium alloy	Polished	Yes	Free flight
	73.25	Magnesium alloy	Polished	Yes	

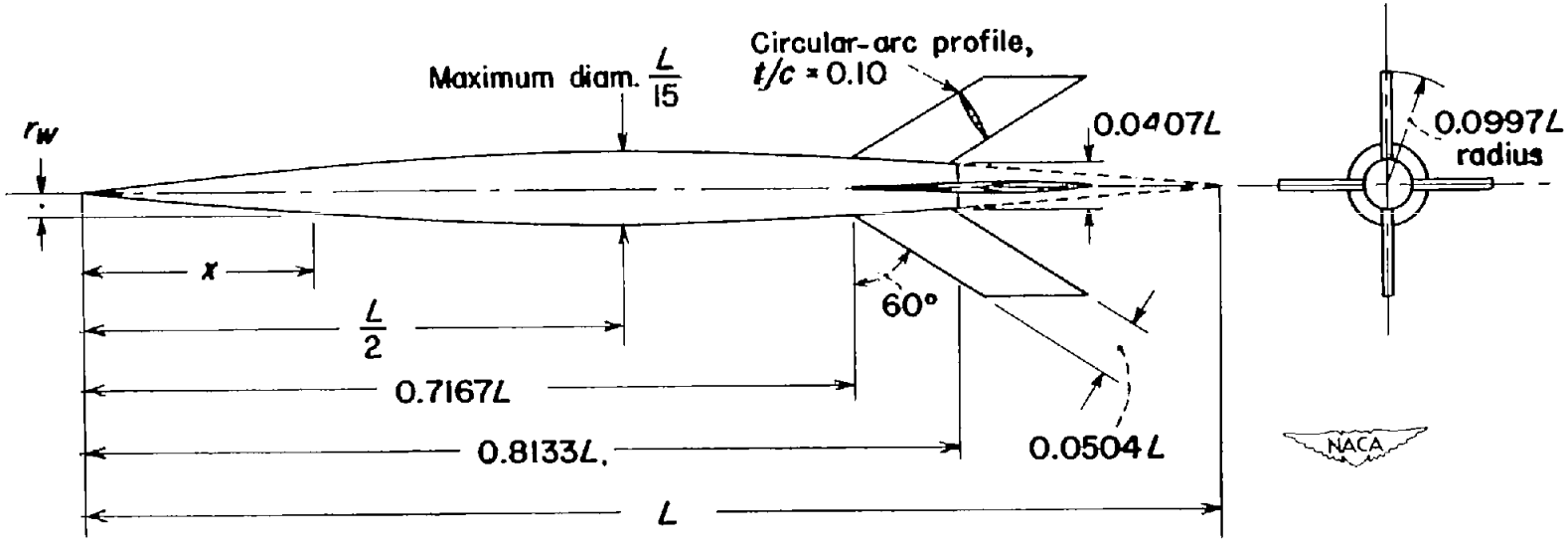

Figure 1.- General configuration of RM-10 research model. Body profile equation, $r_w = \frac{x}{7.5}\left(1.0 - \frac{x}{L}\right)$.

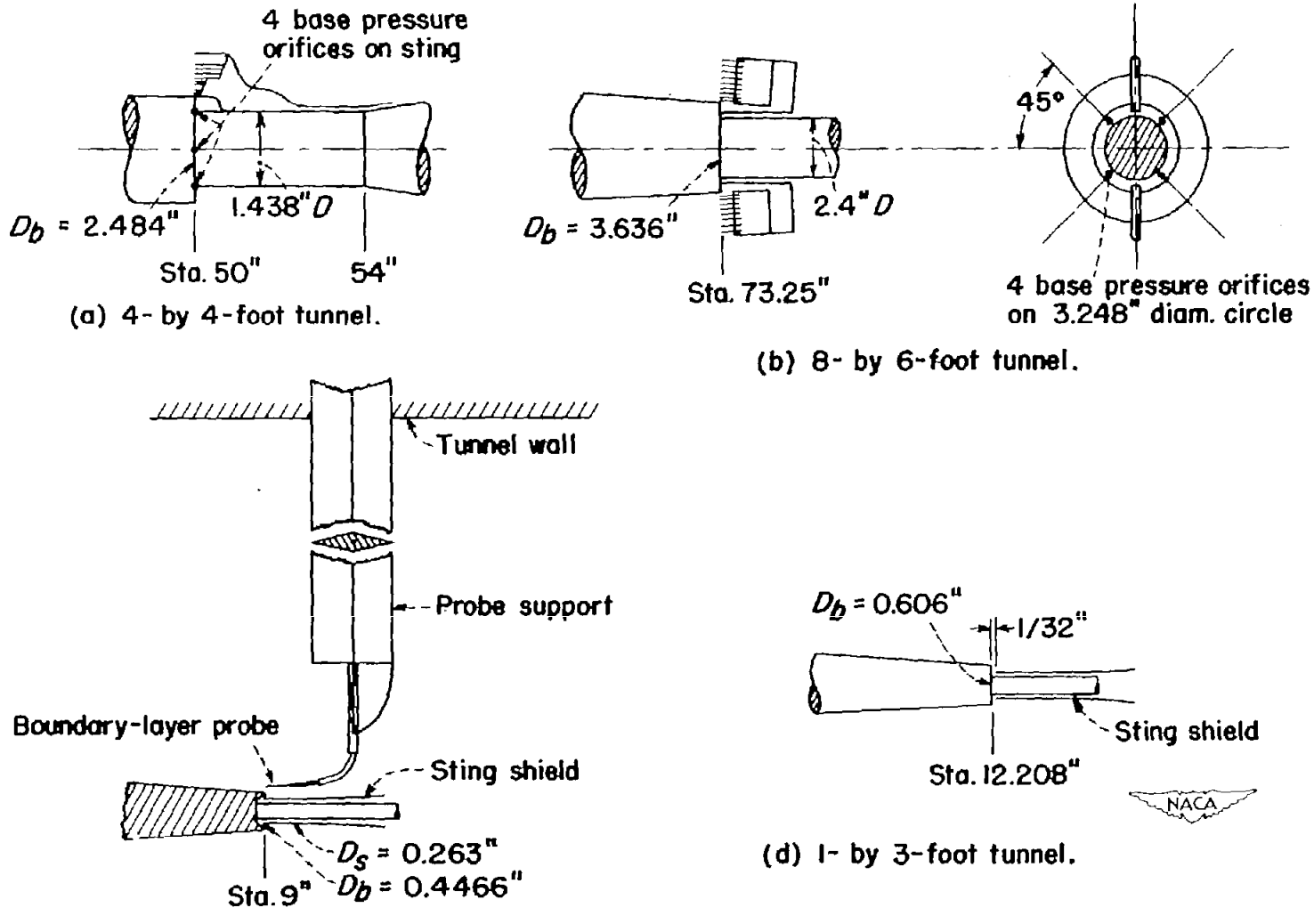

Figure 2.- Instrumentation at base of tunnel models.

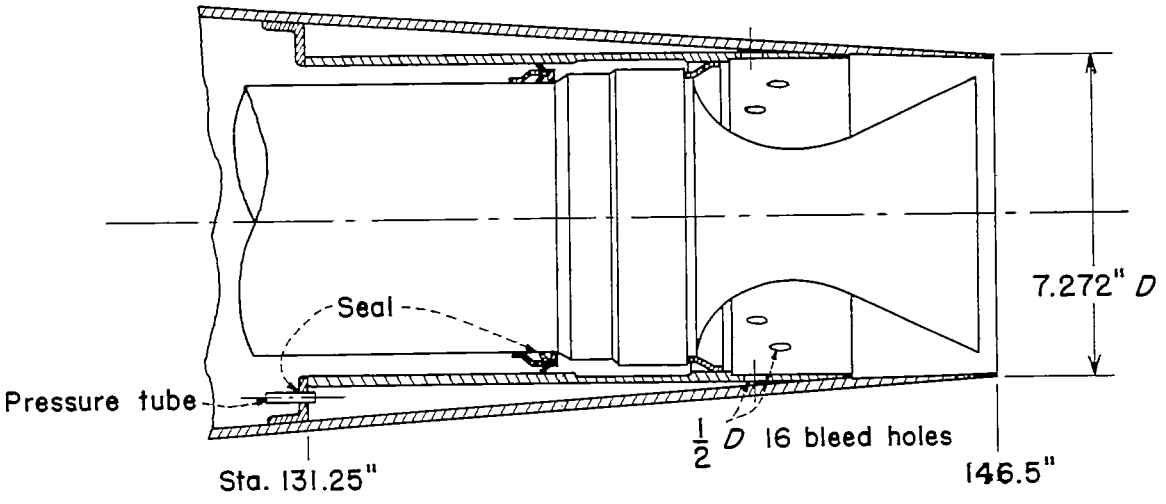

(a) Model 1.

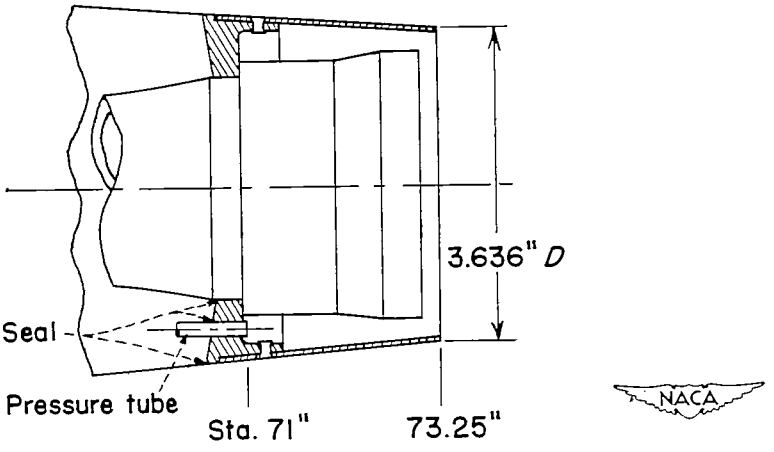

(b) Models A, B, C, E.

Figure 3.- Instrumentation and details of bases of flight models.

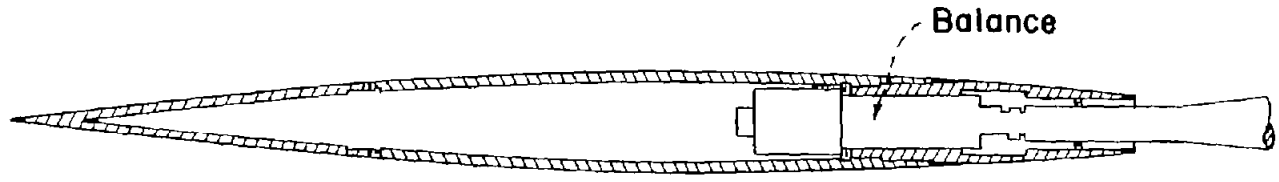

(a) Internal strain-gage balance; 4- by 4-foot tunnel (representative of arrangement in 8- by 6-foot tunnel).

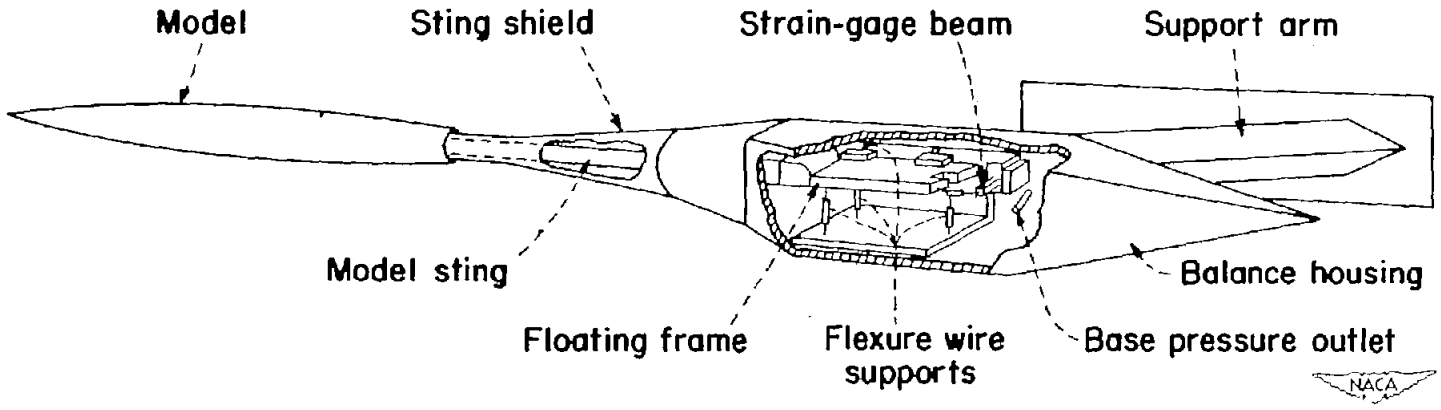

(b) Strain-gage balance external to model; 9-inch tunnel (representative of arrangement in 1- by 3-foot tunnel).

Figure 4.- Sketch of model mounting and internal and external balance systems.

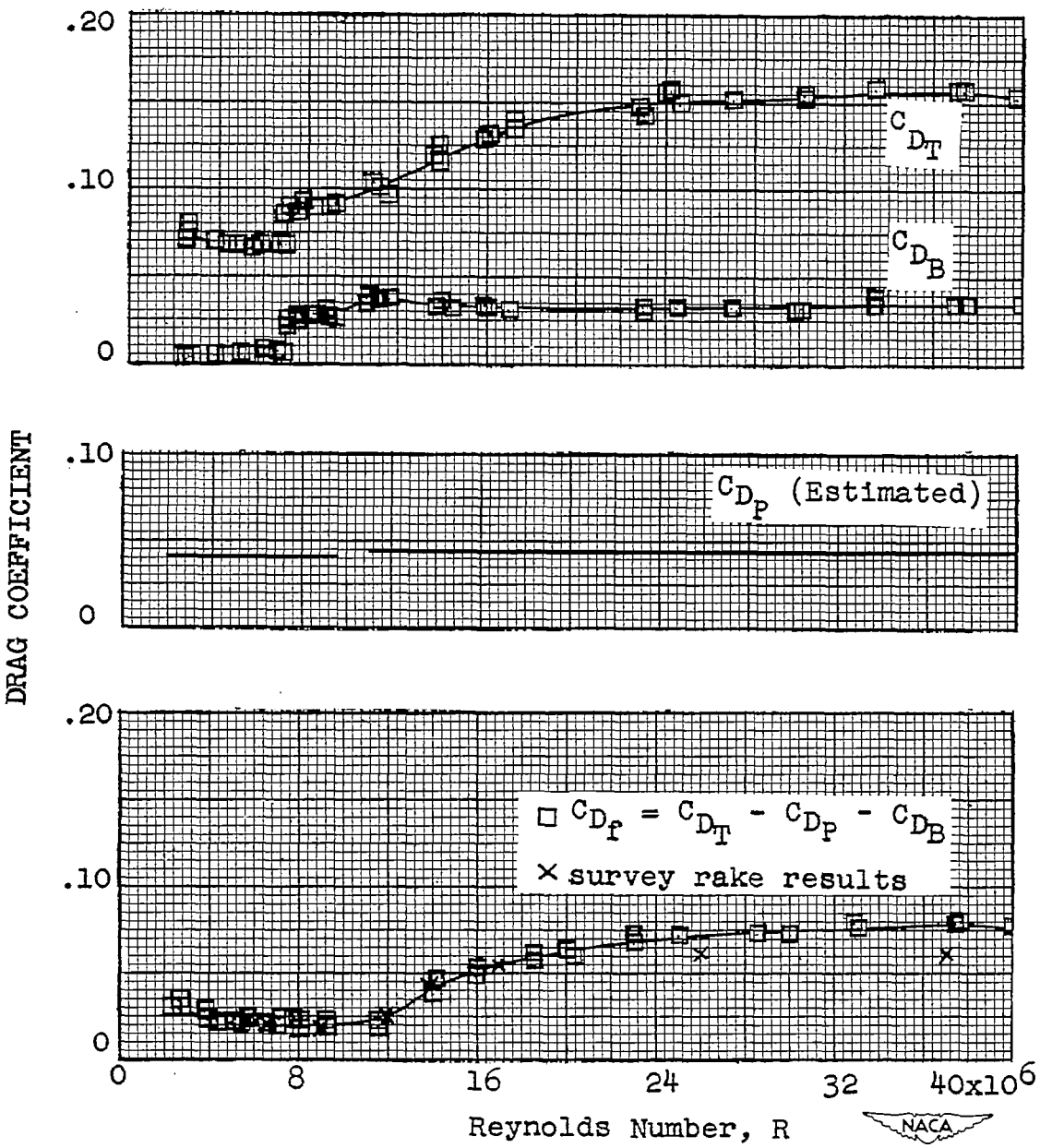

(a) Natural transition.

Figure 5.- Variation of drag coefficient with Reynolds number. 4- by 4-foot tunnel. Body alone. $M = 1.6$; $\alpha = 0^\circ$.

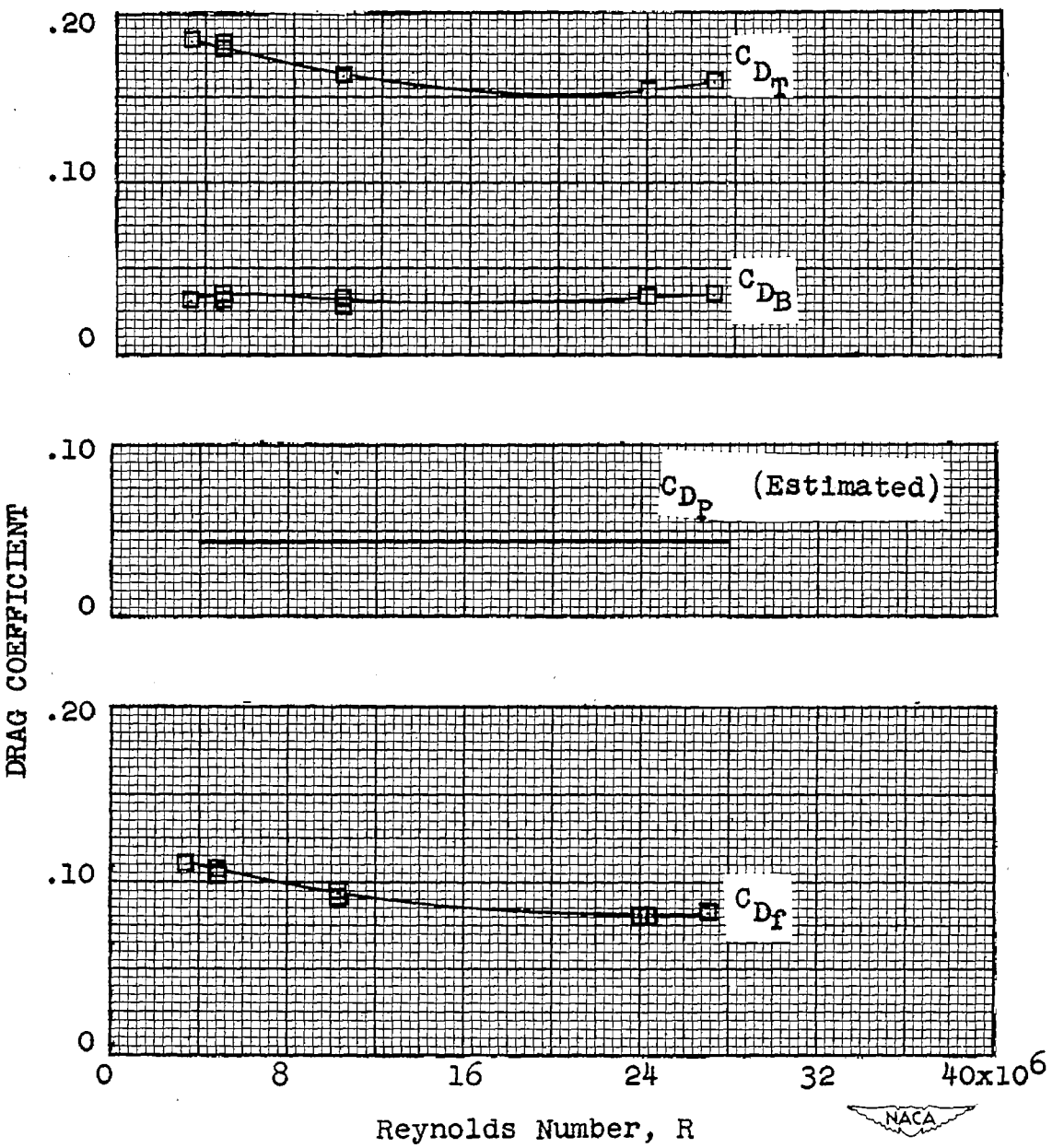

(b) Transition fixed near body nose.

Figure 5.- Concluded.

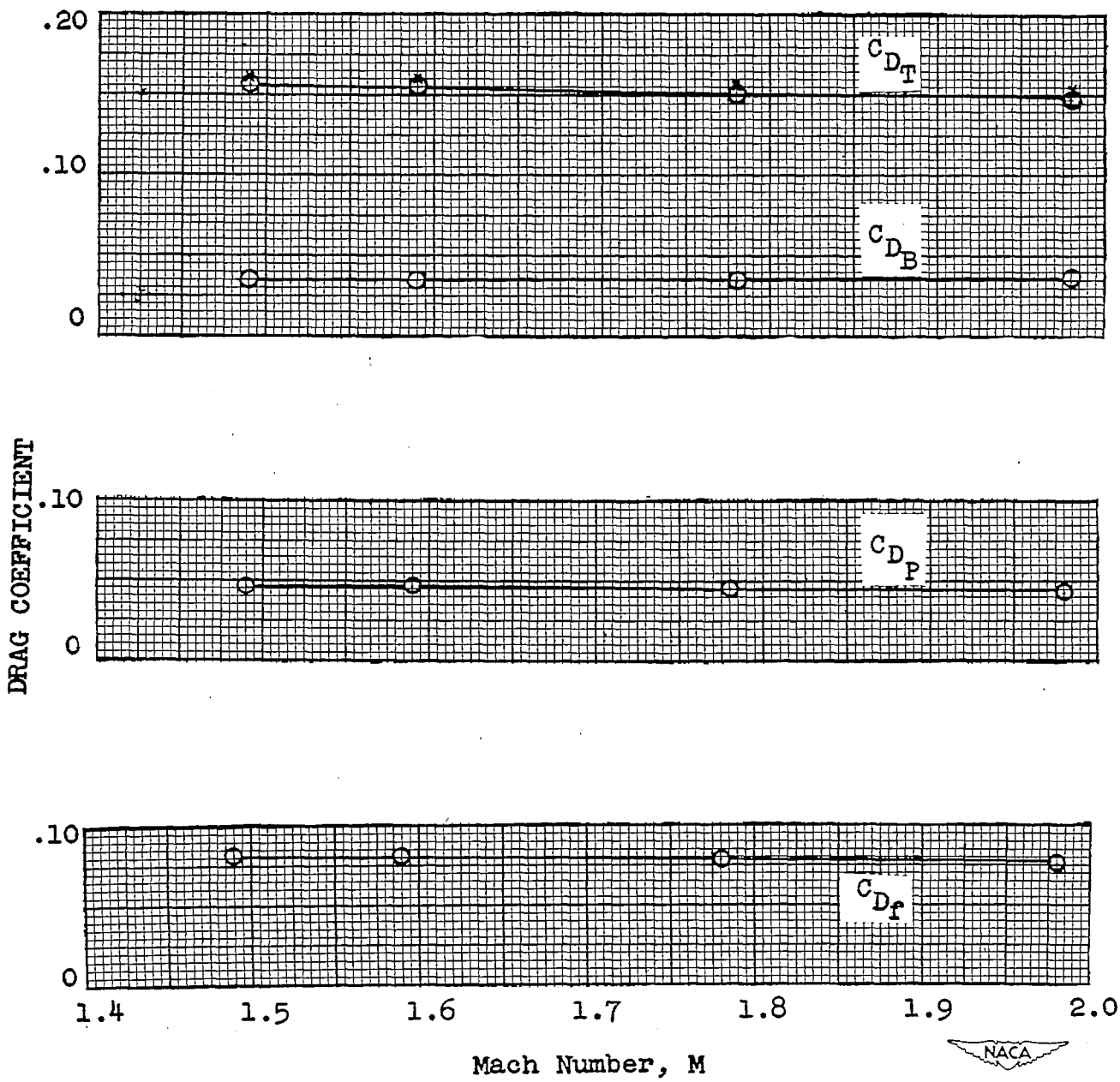

Figure 6.- Variation of drag coefficient with Mach number. 8- by 6-foot tunnel. Body alone. $R \approx 30 \times 10^6$; $\alpha = 0^\circ$. Natural transition.

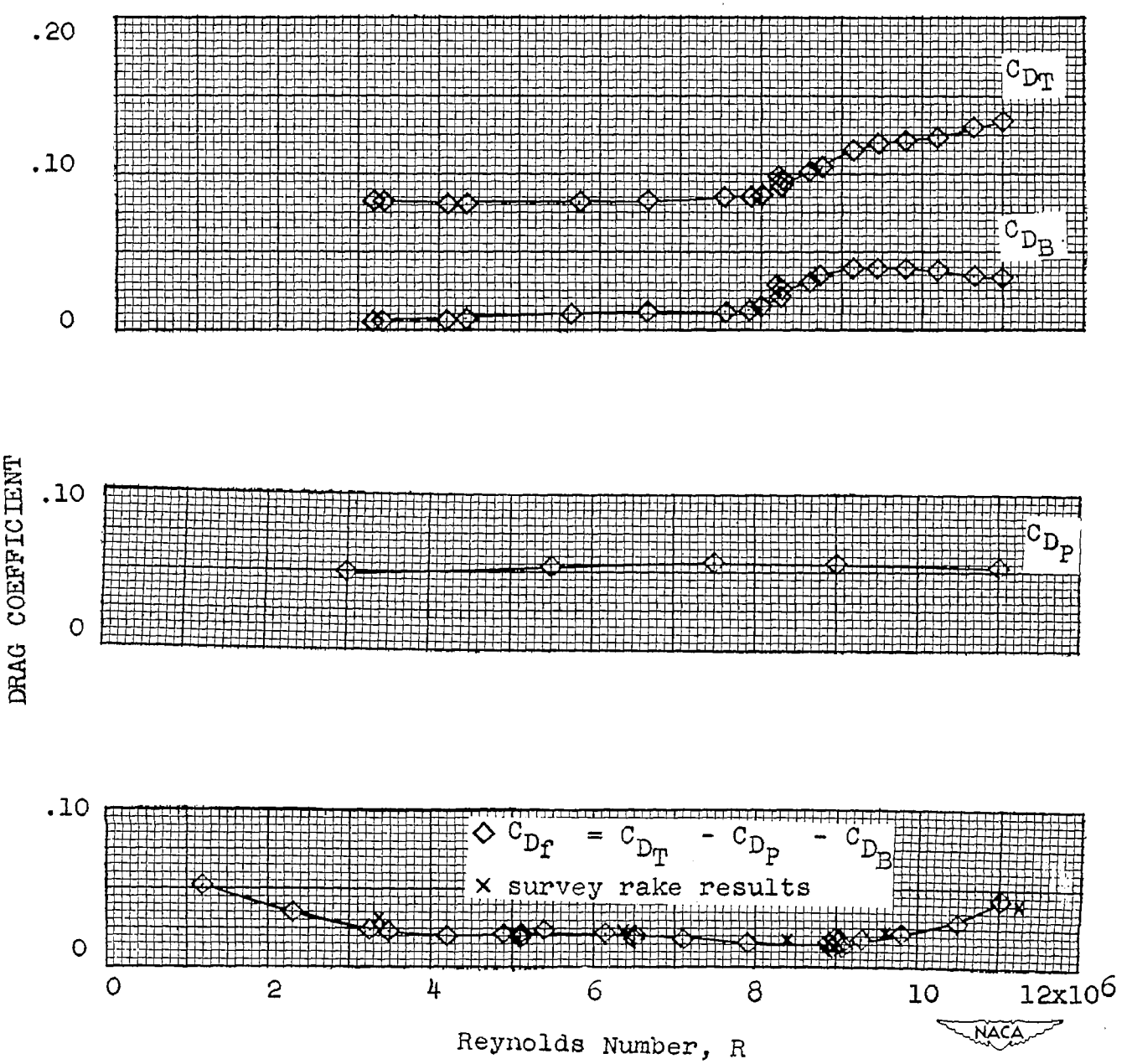

(a) M = 1.62; natural transition.

Figure 7.- Variation of drag coefficient with Reynolds number. 9-inch tunnel. Body alone. $\alpha = 0°$.

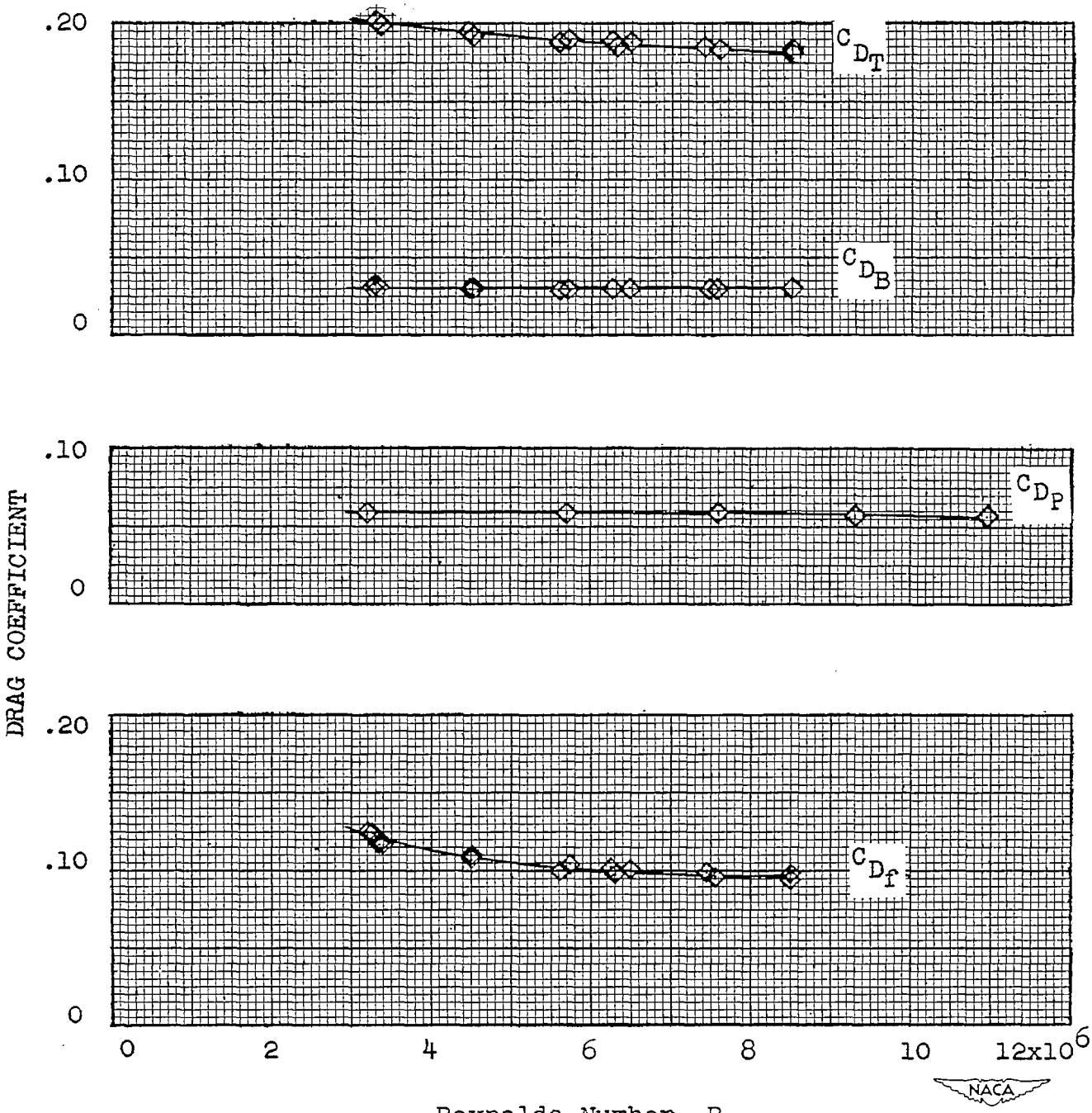

(b) M = 1.62; transition fixed near body nose.

Figure 7.- Continued.

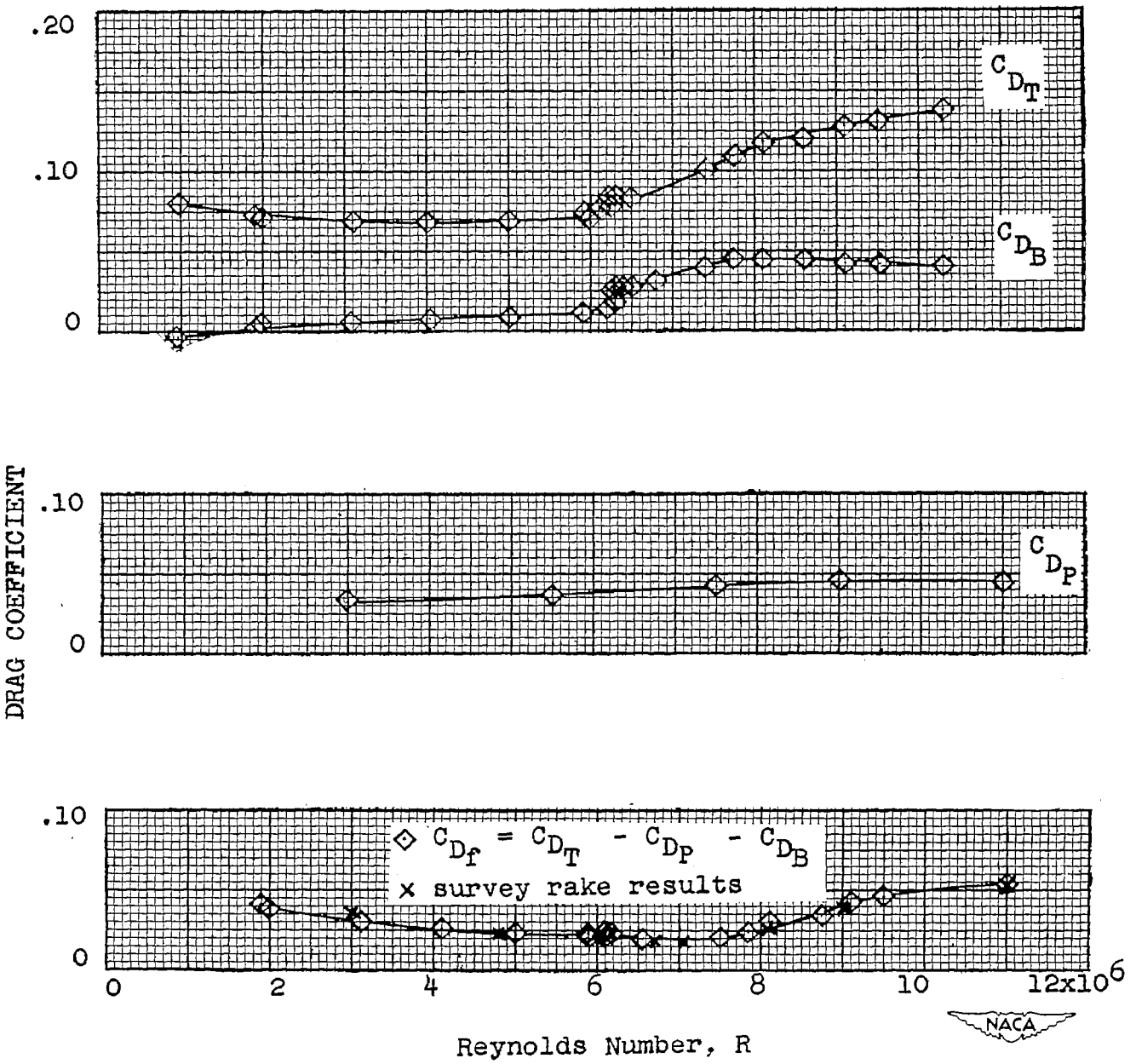

(c) M = 1.93; natural transition.

Figure 7.- Continued.

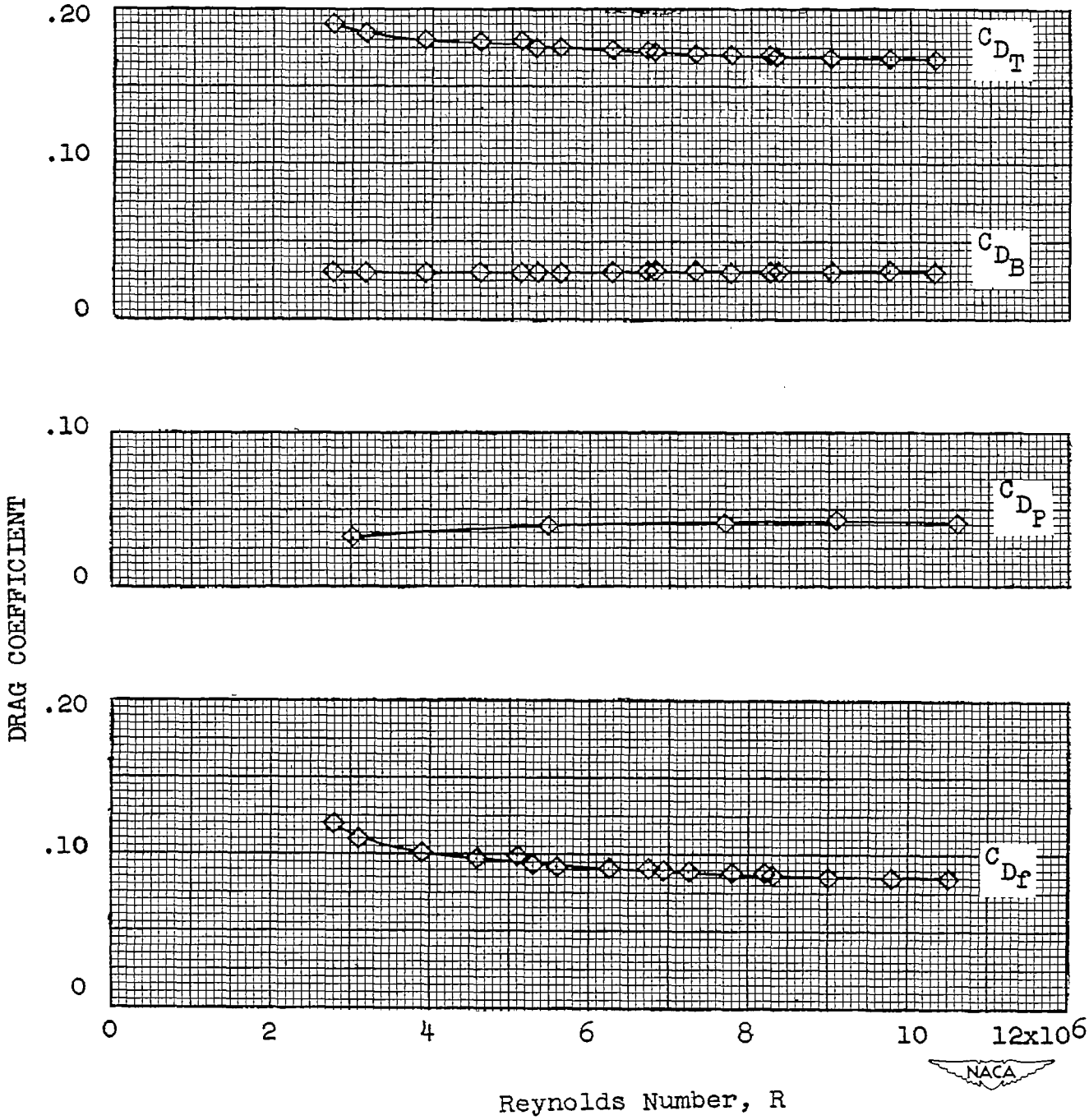

(d) M = 1.93; transition fixed near body nose.

Figure 7.- Continued.

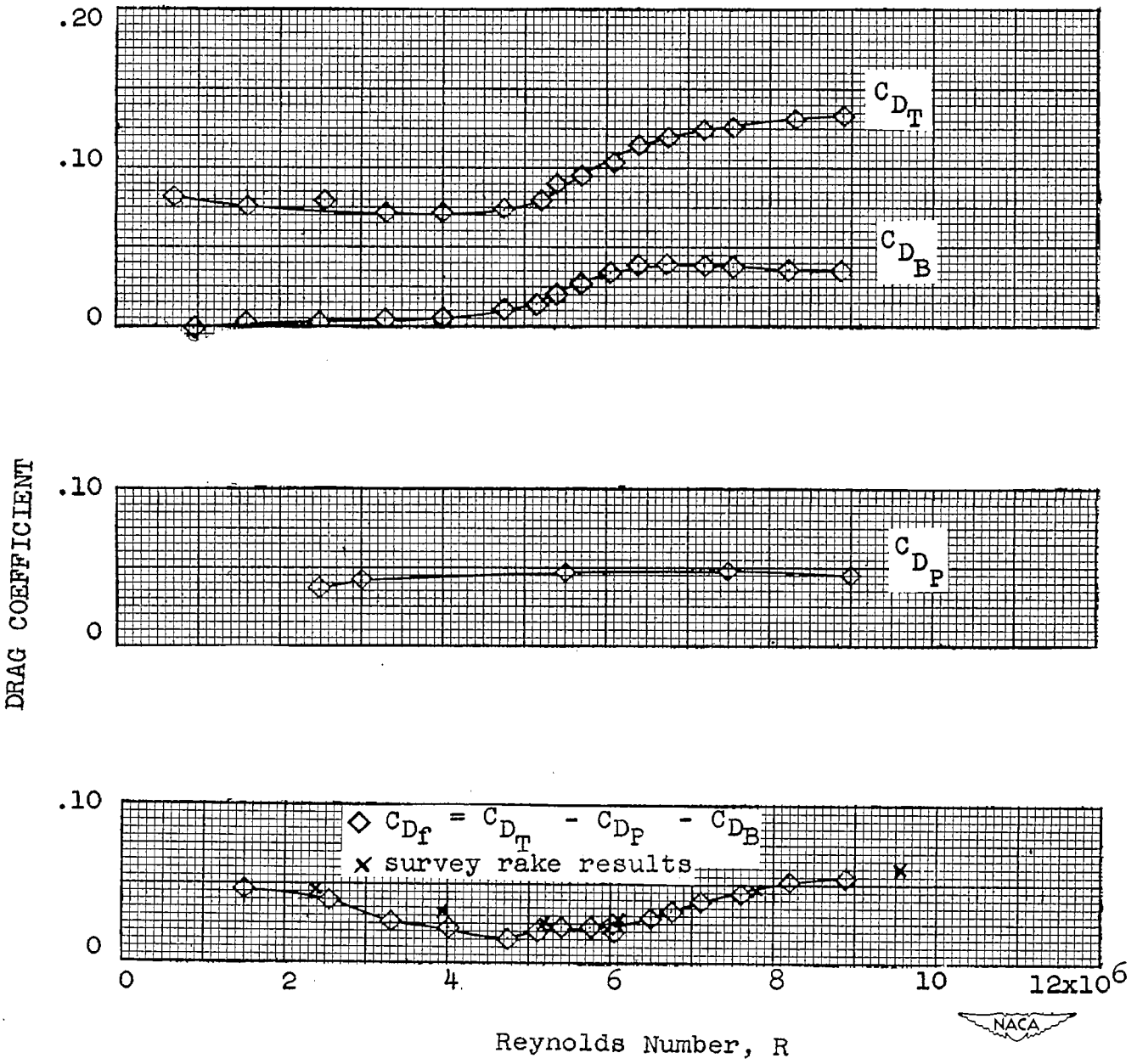

(e) M = 2.41; natural transition.

Figure 7.- Continued.

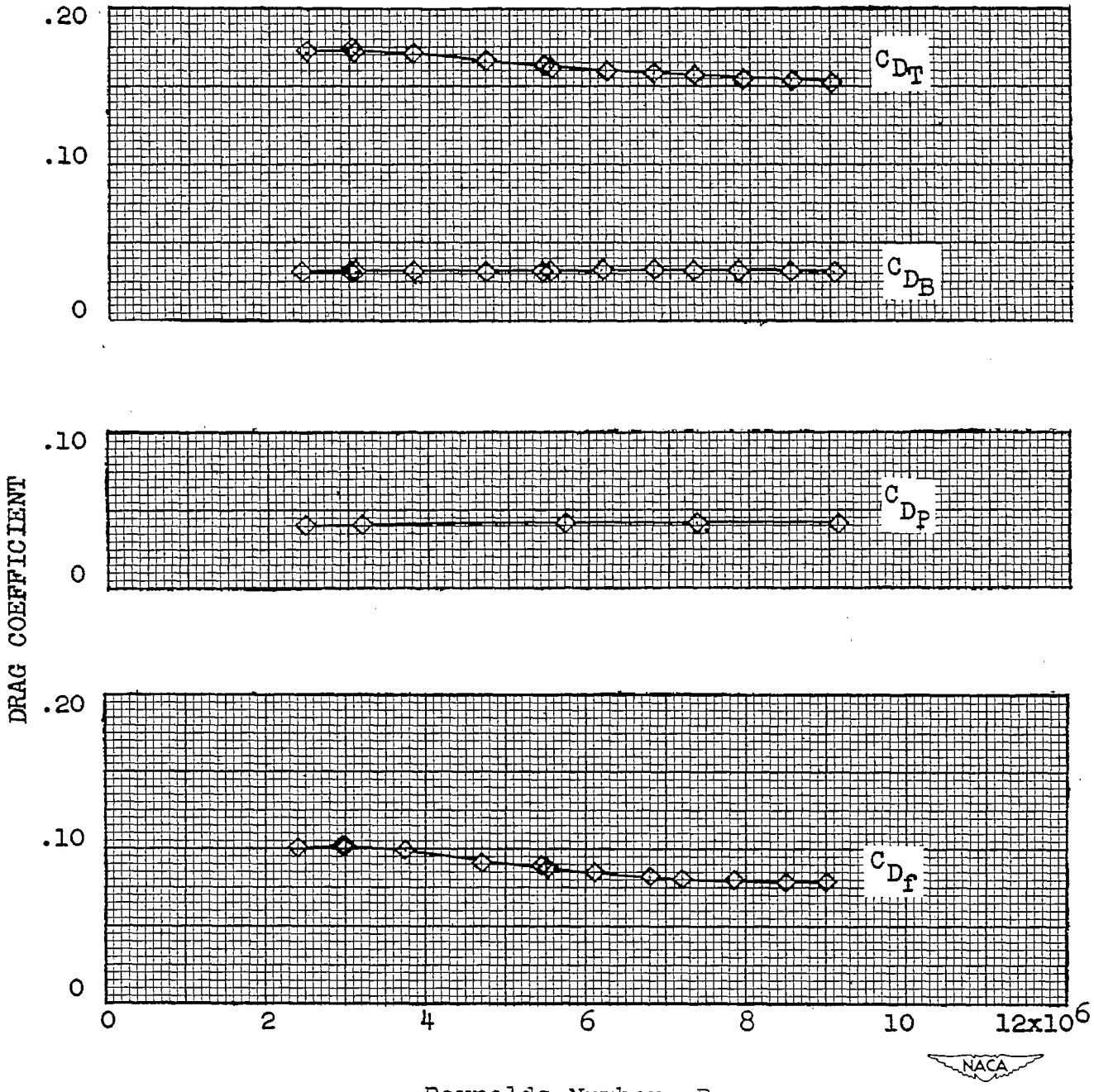

(f) M = 2.41; transition fixed near body nose.

Figure 7.- Concluded.

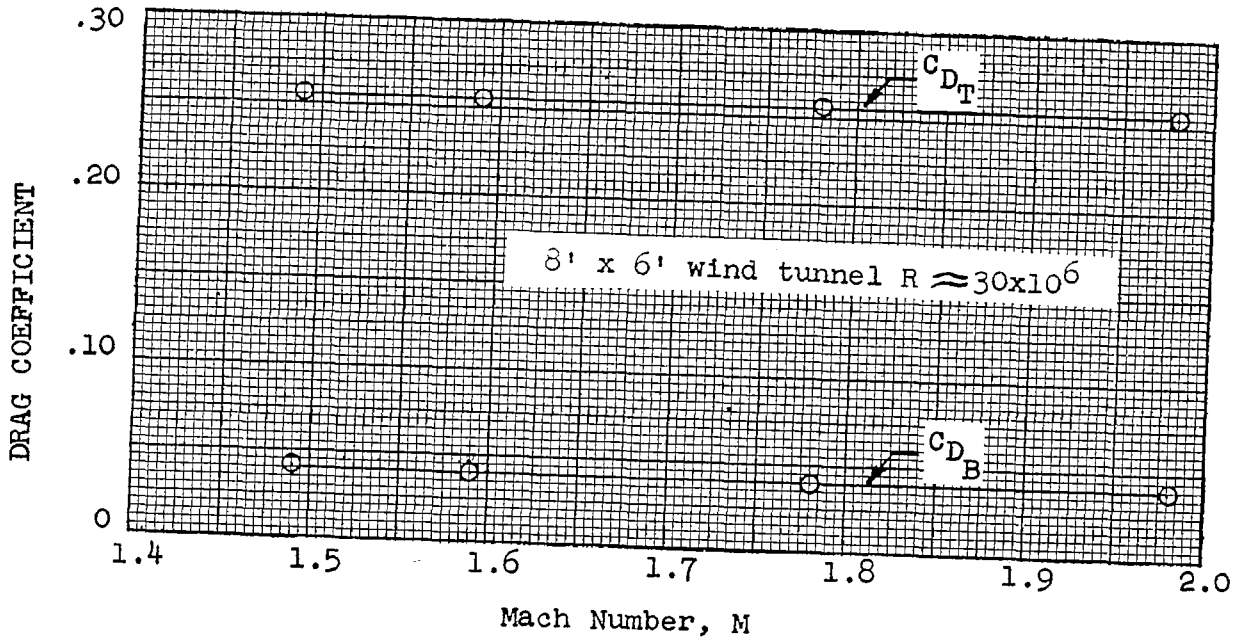

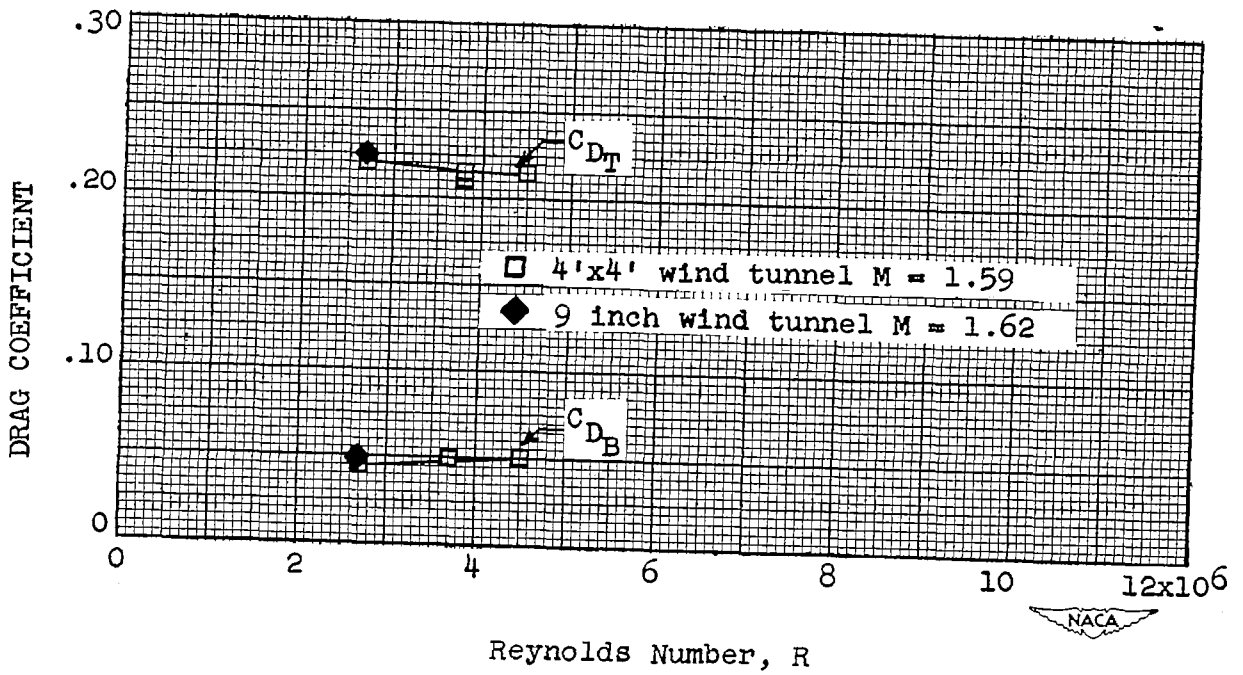

Figure 8.- Drag coefficient from wind-tunnel tests for body with four fins. $\alpha = 0^{\circ}$. Natural transition.

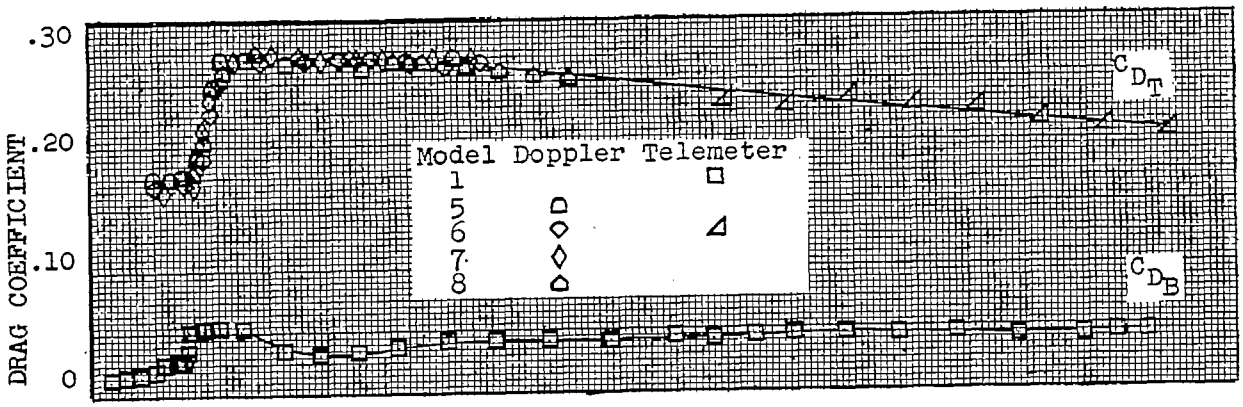

(a) Model length, 146.5 inches.

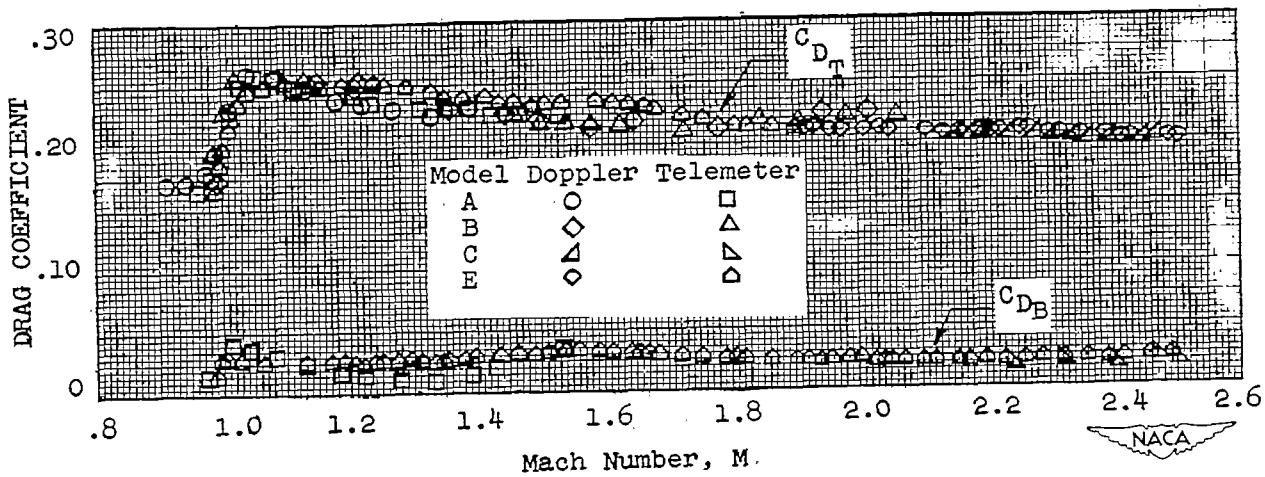

(b) Model length, 73.25 inches.

Figure 9.- Variation of drag coefficient with Mach number for flight models. $\alpha = 0^\circ$.

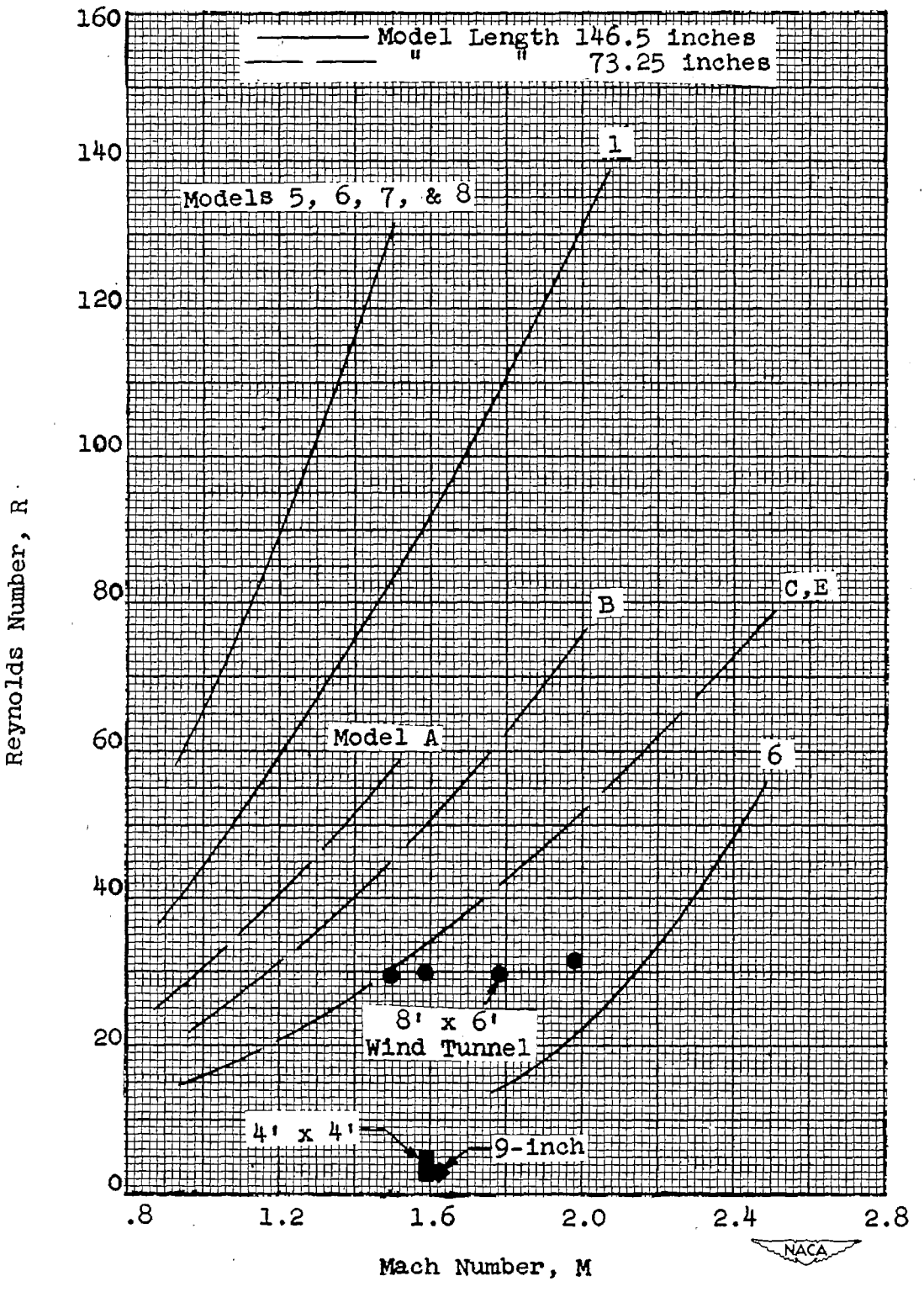

Figure 10. Variation of Reynolds number with Mach number for flight models.

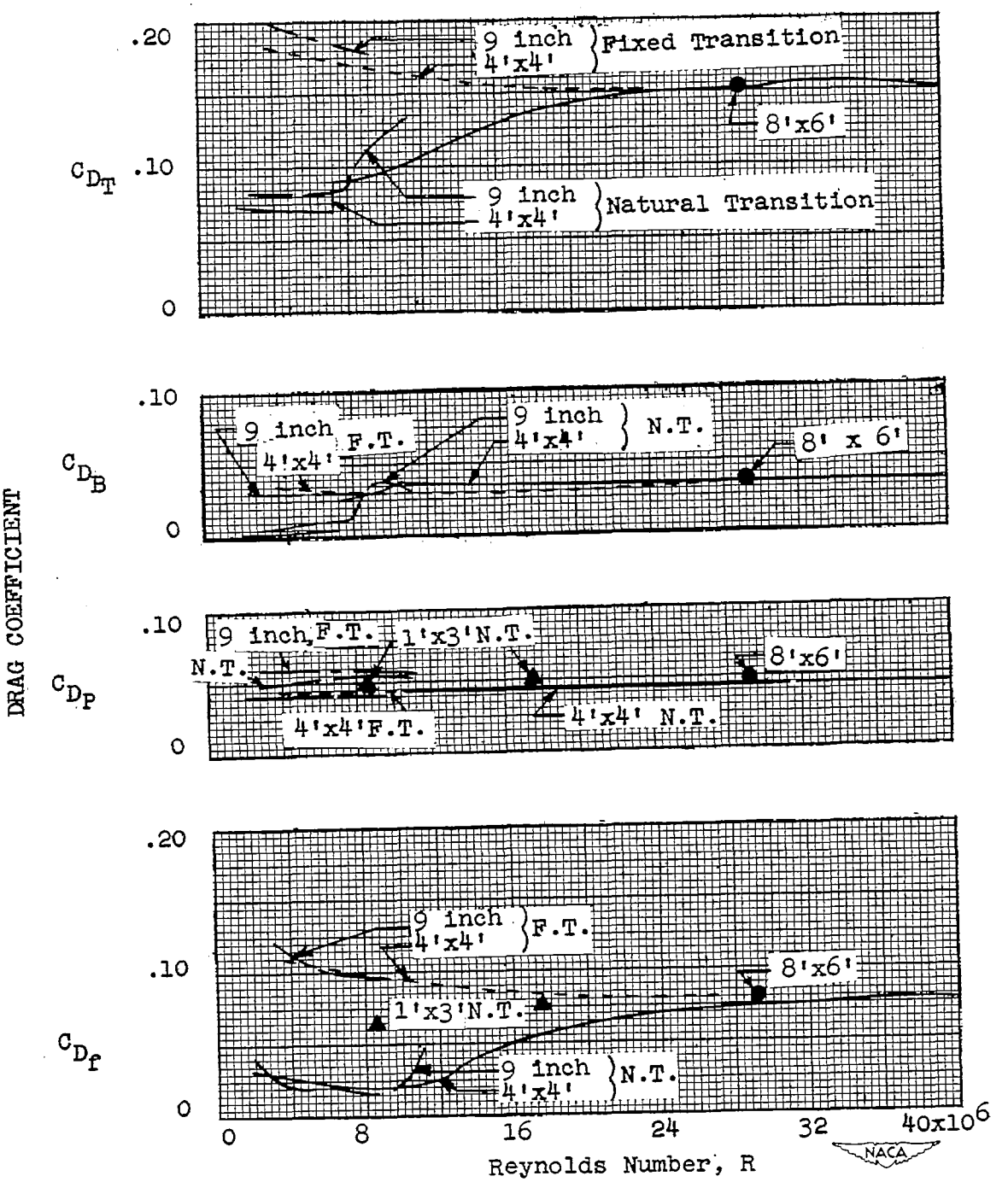

(a) $M \approx 1.6$.

Figure 11.- Comparison of variation of wind-tunnel results with Reynolds number for body alone. $\alpha = 0^\circ$.

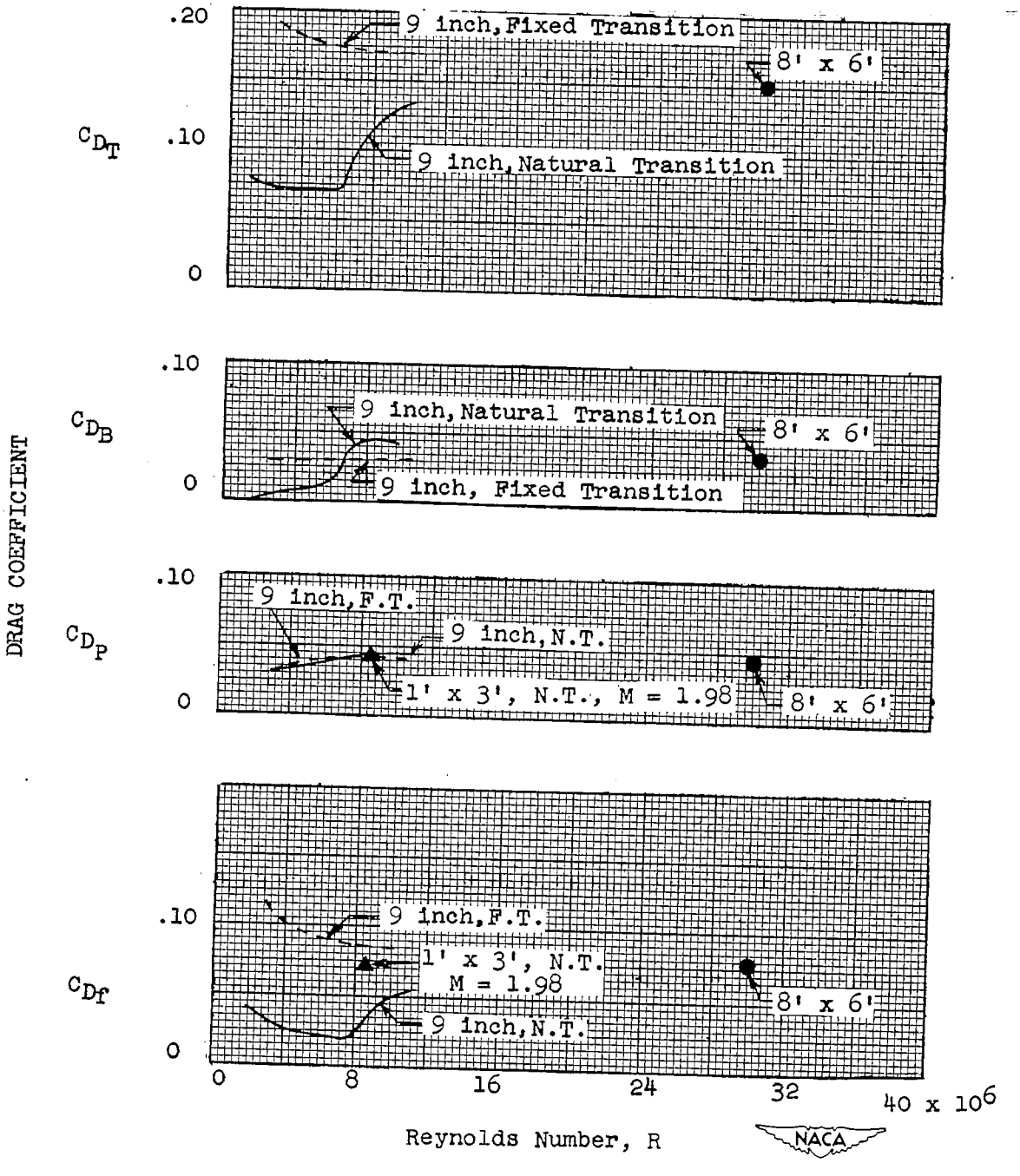

(b) M = 1.93.

Figure 11.- Concluded.

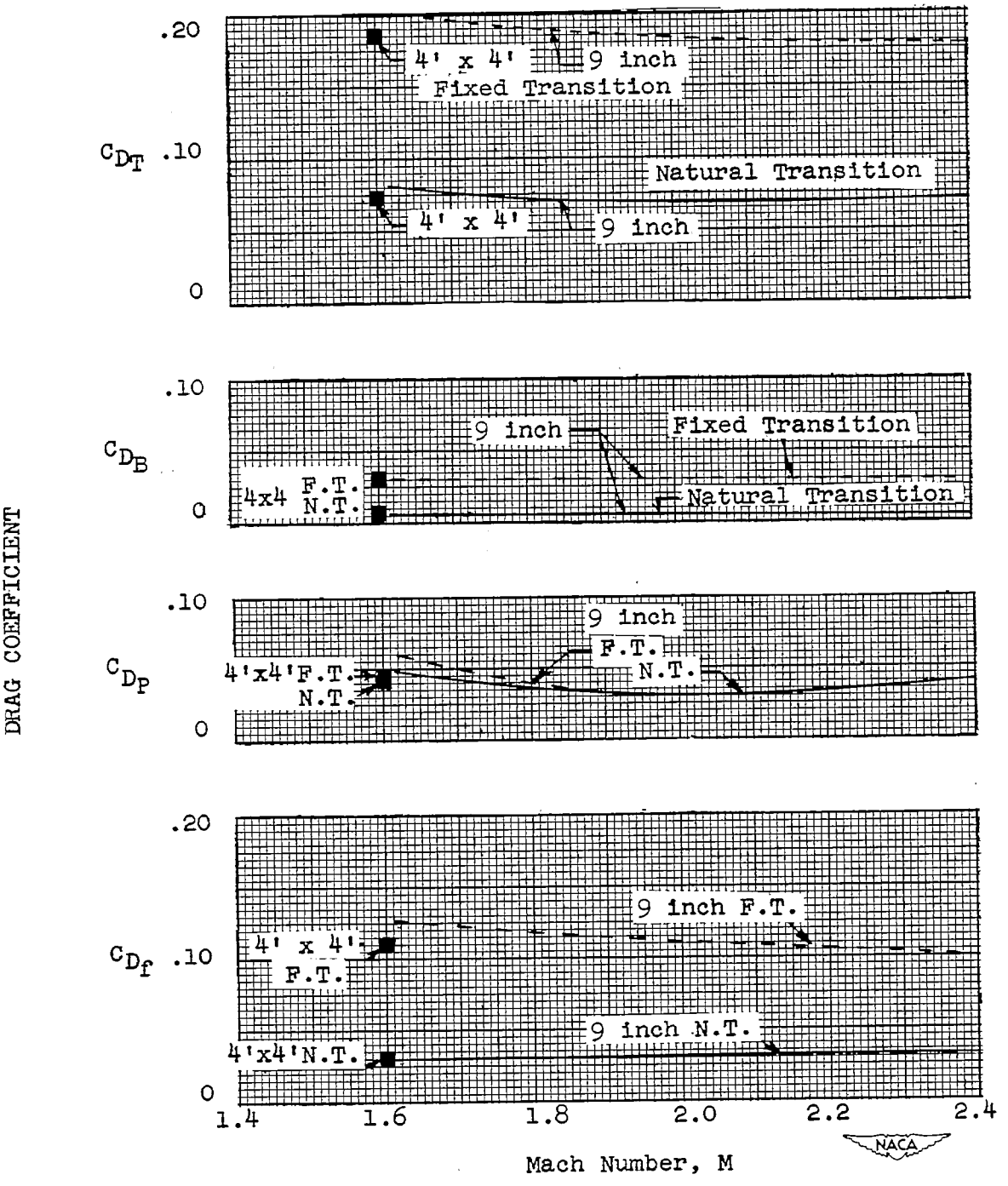

(a) $R = 3 \times 10^6$.

Figure 12.- Comparison of variation of wind-tunnel results with Mach number for body alone. $\alpha = 0^\circ$.

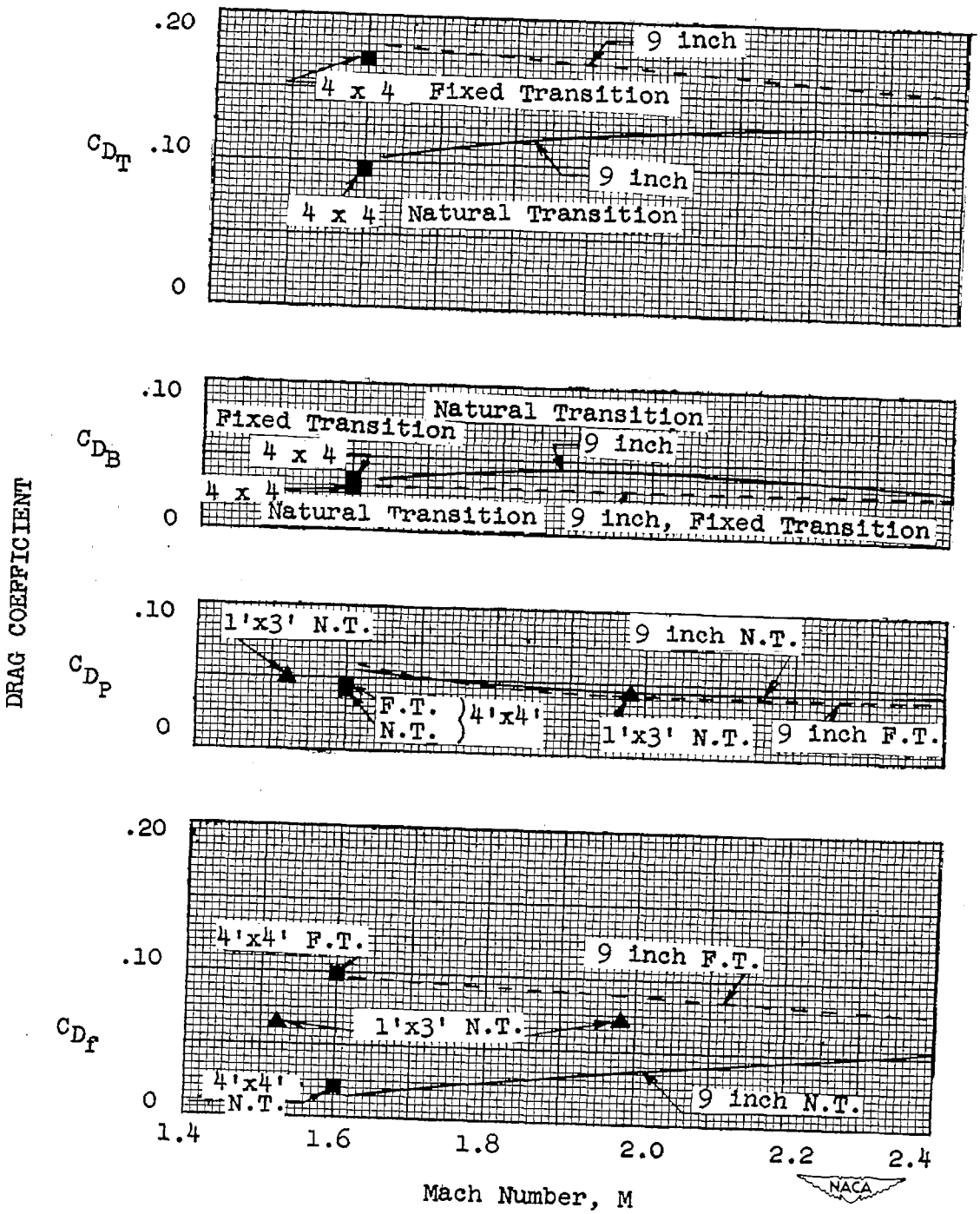

(b) $R = 8.6 \times 10^6$.

Figure 12.- Continued.

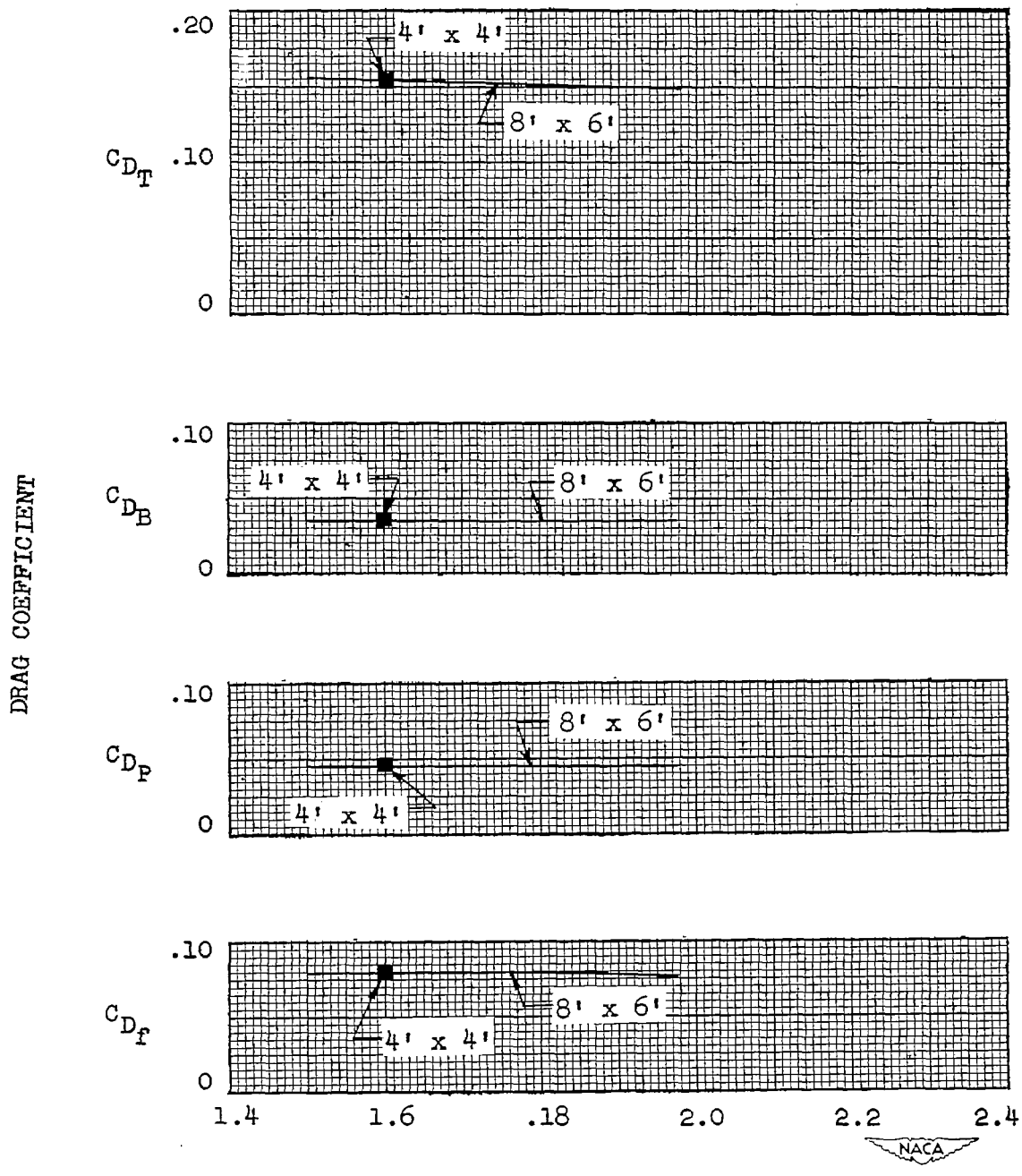

(c) $R \approx 30 \times 10^6$.

Figure 12.- Concluded.

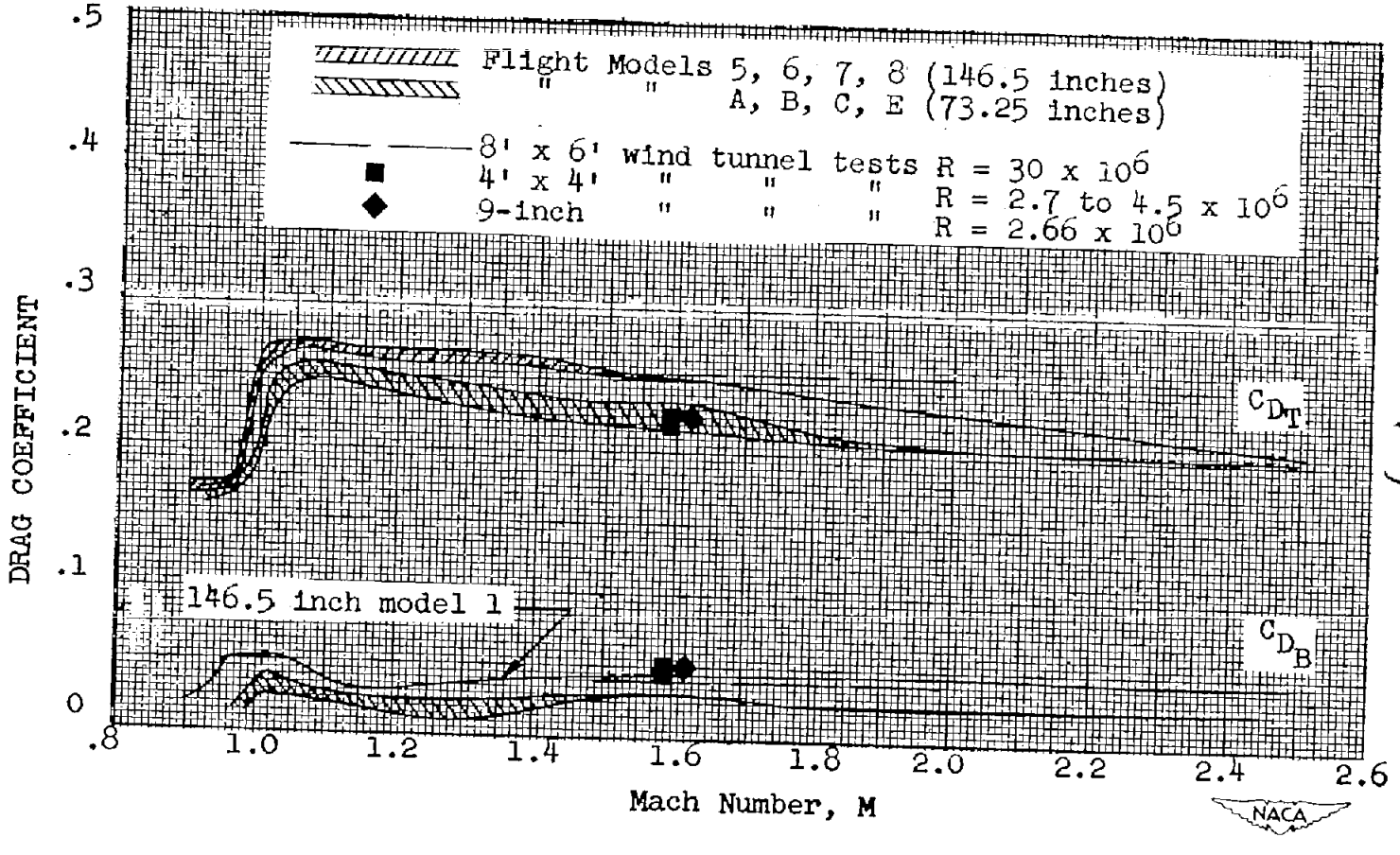

Figure 13.- Comparison of wind-tunnel and flight results for body with four fins. $\alpha = 0^{\circ}$.